Progress in Biophysics and Molecular Biology 115 (2014) 129–139

Contents lists available at ScienceDirect

Progress in Biophysics and Molecular Biology

journal homepage: www.elsevier.com/locate/pbiomolbio

Review

Relevance of cardiomyocyte mechano-electric coupling to stretch-induced arrhythmias: Optical voltage/calcium measurement in mechanically stimulated cells, tissues and organs

Kinya Seo [a], Masashi Inagaki [b], Ichiro Hidaka [c], Hana Fukano [d], Masaru Sugimachi [b], Toshiaki Hisada [d], Satoshi Nishimura [e, f], Seiryo Sugiura [d, *]

[a] Division of Cardiology, Department of Medicine, The Johns Hopkins Medical Institutions, Baltimore, MD 21205, USA
[b] Department of Cardiovascular Dynamics, National Cerebral and Cardiovascular Center Research Institute, Osaka 565-0873, Japan
[c] Division of Physical and Health Education, Graduate School of Education, The University of Tokyo, Tokyo 113-0033, Japan
[d] Department of Human and Engineered Environmental Studies, Graduate School of Frontier Sciences, The University of Tokyo, 5-1-5 Kashiwanoha, Kashiwa, Chiba 277-8563, Japan
[e] Research Division of Cell and Molecular Medicine, Center for Molecular Medicine, Jichi Medical University, Tochigi 329-0498, Japan
[f] Department of Cardiovascular Medicine, Translational Systems Biology and Medicine Initiative, The University of Tokyo, Tokyo 113-8655, Japan

ARTICLE INFO

Article history:
Available online 30 July 2014

Keywords:
Mechano-electric coupling
Stretch-induced arrhythmia
Commotio cordis
Carbon-fiber
Optical mapping
Optical trap

ABSTRACT

Stretch-induced arrhythmias are multi-scale phenomena in which alterations in channel activities and/or calcium handling lead to the organ level derangement of the heart rhythm. To understand how cellular mechano-electric coupling (MEC) leads to stretch-induced arrhythmias at the organ level, we developed stretching devices and optical voltage/calcium measurement techniques optimized to each cardiac level. This review introduces these experimental techniques of (1) optical voltage measurement coupled with a carbon-fiber technique for single isolated cardiomyocytes, (2) optical voltage mapping combined with motion tracking technique for myocardial tissue/whole heart preparations and (3) real-time calcium imaging coupled with a laser optical trap technique for cardiomyocytes. Following the overview of each methodology, results are presented. We conclude that individual MEC in cardiomyocytes can be heterogeneous at the ventricular level, especially when moderate amplitude mechanical stretches are applied to the heart, and that this heterogeneous MEC can evoke focal excitation that develops into re-entrant arrhythmias.

Contents

* Corresponding author. Tel.: +81 3 5841 8393; fax: +81 3 5841 6376.
E-mail addresses: seokin54@gmail.com (K. Seo), masashi@ncvc.go.jp (M. Inagaki), hidaka@p.u-tokyo.ac.jp (I. Hidaka), hanaff87@gmail.com (H. Fukano), su91mach@ncvc.go.jp (M. Sugimachi), hisada@mech.t.u-tokyo.ac.jp (T. Hisada), snishi-tky@umin.ac.jp (S. Nishimura), sugiura@k.u-tokyo.ac.jp (S. Sugiura).

http://dx.doi.org/10.1016/j.pbiomolbio.2014.07.008
0079-6107/

1. Introduction

Alterations in the mechanical state of the heart can affect its electrophysiological behavior (Kohl et al., 2011; Ravens, 2003; Taggart and Lab, 2008). This mechano-electric coupling (MEC) is considered to play an important role in cardiac rhythm abnormalities, especially in disease states such as old myocardial infarction and chronic heart failure, in which ventricular walls are subjected to abnormal hemodynamic loading stresses (Aimond et al., 1999; Janse, 2004; Tomaselli and Marban, 1999). Sudden mechanical impact to the heart can also disarrange the heart rhythm even in healthy subjects, which in some instances leads to sudden cardiac death (Link, 2012). However, this phenomenon (termed *commotio cordis*) is rare, and evidence linking mechanical impact to fatal arrhythmias is scarce.

The mechanisms underlying MEC relate to the activation of ion channels by mechanical stretch (Sachs, 2010, 2011). Because such stretch-activated channels (SACs) have long been suspected as important contributors to MEC, there are many reports on characterization of these channels (Bett and Sachs, 2000; Craelius et al., 1988; Kohl et al., 1998; Niu and Sachs, 2003; Ward et al., 2008). In particular, considering the physiological loading conditions for each myocyte in the ventricular wall, numerous studies have been performed in isolated cardiomyocytes in response to axial stretching to elucidate the properties of SACs (Belus and White, 2003; Iribe et al., 2010; Kamkin et al., 2003; Riemer and Tung, 2003; Sasaki et al., 1992; Zeng et al., 2000). However, single channel recording in the stretch-imposed ventricular myocytes demands technical proficiency because of the difficulty in maintaining stable attachment of the glass electrode during the stretch. These restrictions also impair the ability to study the dynamic properties of cellular MEC induced by transient mechanical stretches.

Recent studies have revealed that axial stretching of cardiomyocytes enhances Ca^{2+} spark/wave rate via mechanisms dependent on microtubule-mediated modulation (Iribe et al., 2009), NADPH2 oxidase (NOX2) activation (Prosser et al., 2011) and neuronal nitric oxide synthase (nNOS) activation (Jian et al., 2014) of the ryanodine receptor. On the one hand, stretch acutely increases the affinity of troponin C to Ca^{2+} (Allen and Kentish, 1988), so that when stretched tissue is released there is a surge in intracellular Ca^{2+}, which can lead to Ca^{2+} waves (ter Keurs et al., 2008). These spontaneous Ca^{2+} releases are regarded as an important substrate for triggered arrhythmias and delayed after depolarizations (Fujiwara et al., 2008), though whether SACs and/or Ca^{2+} cycling contributes to MEC-related arrhythmias is unclear.

To clarify how MEC contributes to ventricular arrhythmias, various studies have been performed with cardiac tissues and whole heart preparations (Fasciano and Tung, 1999; Franz et al., 1992; Hansen et al., 1990; Parker et al., 2001). However, many of these reports are limited owing to lack of experimental methodologies for recording the electrical and mechanical activity simultaneously and with high spatiotemporal resolution. For instance, optical mapping (Efimov et al., 2004; Herron et al., 2012), a technique used to examine spatiotemporal electrical behavior in the heart, often necessitates either physically or pharmacologically constraining the heart contraction, which limits its utility for MEC research.

Herein, we review our techniques that we developed to resolve these various methodological issues in isolated cardiac myocytes (Section 2) and myocardial tissues (Section 3). Next, we discuss a possible scenario for the link between cellular MEC and fatal arrhythmias (Section 4). Furthermore, we briefly introduce our ongoing studies using an optical trap technique to elucidate the mechanisms of stretch-mediated Ca^{2+} handling (Section 5), and then provide a final conclusion (Section 6).

2. Cardiomyocyte study

There are only a small number of studies reporting the characteristics of cardiomyocytes MEC upon axial stretching. Considering the dynamic changes in stress and strain that an individual cardiomyocyte experiences in the beating heart, it is important to examine the responses to dynamic stretching on single cardiomyocytes. In this section, we introduce our methodology for examining single cardiomyocytes, in which we combine a carbon-fiber technique with optical voltage measurement for assessing cellular MEC upon dynamic stretching.

2.1. Carbon-fiber technique for single cardiomyocyte stretching

Single adult cardiomyocytes have been widely used to relate subcellular molecular events to functional characteristics of the heart. The simple geometry of a myocyte offers substantial advantages over multicellular preparations due to the fairly homogeneous strain distribution and exogenous factors (Palmer et al., 1996; Yasuda et al., 2001). However, they are notoriously difficult to manipulate and maintain because of the irritability and fragility of the sarcolemma. A number of techniques have been proposed to overcome these limitations. For example, Kamkin applied local stretches to ventricular myocytes by pulling with a glass stylus and patch-pipette (Kamkin et al., 2000), while Zeng and Riemer used a pair of suction pipettes to pull the myocyte from each end (Riemer and Tung, 2003; Zeng et al., 2000). A totally different technique was introduced by Le Guennec (Le Guennec et al., 1990) in which a pair of thin carbon fibers was attached to the myocyte surface, likely because of electrostatic forces between the fibers and the surface (Garnier, 1994). This technique was later modified with the use of graphite-reinforced carbon (GRC; Tsukuba Material Information Laboratory Ltd, Tsukuba, Japan) fiber (Sugiura et al., 2006) and/or biocompatible adhesive (MyoTak; IonOptix, Milton, MA, USA; or World Precision Instruments Inc., Sarasota, FL, USA) (Khairallah et al., 2012; Prosser et al., 2011) to enable firmer attachment between the fibers and the cellular surface, and was used for the dynamic stretching of single cardiomyocytes (Nishimura et al., 2006a, 2006b; Seo et al., 2014).

We typically use a pair of carbon fibers and attach them to each end of a cardiomyocyte to clamp it under a microscope (Sugiura et al., 2006). One fiber is rigid to serve as a mechanical anchor, while the other fiber is compliant and controlled quickly and digitally by a connected piezoelectric transducer (P-841.40; Physik Instrumente, Karlsruhe, Germany). The magnitude of the bending motion of the compliant carbon fiber is monitored by a fast digital dimensioning CCD camera (IonOptix, Milton, MA, USA) (Fig. 1A) to calculate the contractile force by multiplying by the fiber stiffness. The attachment of the carbon fibers to the myocyte surface results

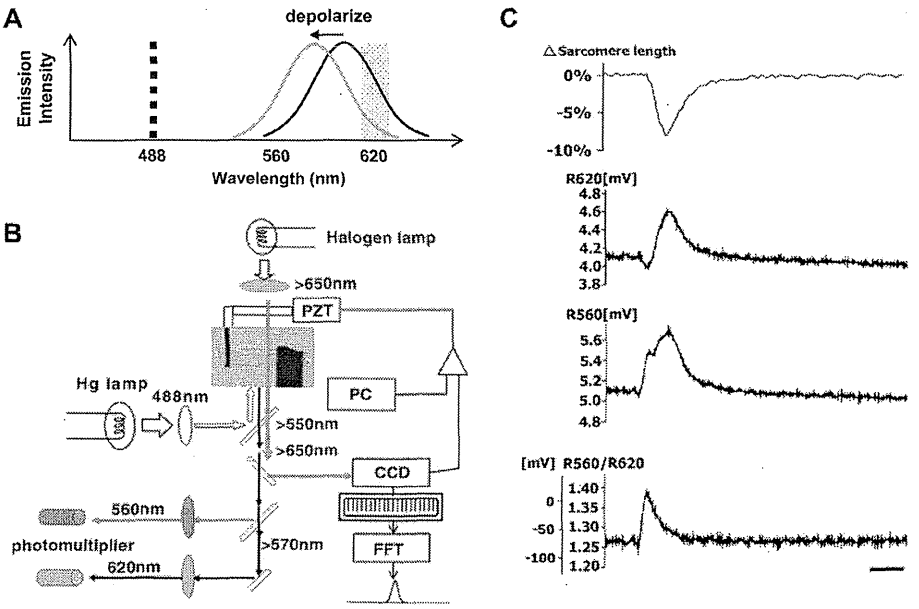

Fig. 1. A) Scheme of the fluorescence properties of di-8-ANEPPS. The dye was excited at 488 nm (dashed line) and two emission lights were detected separately in 560 and 620 nm wavelength bands (shaded boxes). B) Diagram of the experimental setup for cardiomyocyte study. A pair of carbon fibers was attached to the myocyte surface, and the thin fiber was controlled by a piezoelectric translator (PZT) connected to a personal computer (PC). The positions of the carbon fibers were captured by a charge-coupled device camera (CCD), and the sarcomere length was measured by fast Fourier transformation (FFT). For optical voltage measurement, the dye was excited at 488 nm, and the emission light was recorded ratiometrically by two photomultipliers (560 and 620 nm). A long wavelength (>650 nm) was used for the CCD observation. C) Ratiometry of cardiomyocyte action potential. During active contraction indicated by sarcomere shortening, red (620 nm) and green (560 nm) fluorescence signals (raw voltage signals) were recorded with two photomultipliers separately. Ratiometry (R560/R620) successfully removed the motion artifacts. Scale bars: 100 ms.

in minimal damage to the sarcolemma (Cannier et al., 1994) and reduces the need for technical proficiency. Importantly, this technique does not interfere with simultaneous recording of the sarcomere striation and the fluorescent membrane voltage measurement (Nishimura et al., 2006a, 2008) described below.

This carbon-fiber technique can be applied to various experiments with some modifications. For instance, the force–length relationship (Frank-Starling Mechanism) of a single cardiomyocyte can be assessed by measuring contractile force and sarcomere shortening at various stretch levels (Iribe et al., 2007; Nishimura et al., 2004; Scimia et al., 2012; White et al., 1993). Modified techniques were used for assessing slow force responses (Calaghan and White, 2004; Seo et al., 2014) and Ca^{2+} spark/wave rates (Iribe et al., 2009; Prosser et al., 2011) by combining the stretch apparatus with fluorescent calcium measurement. Furthermore, by attaching a latex microsphere to the side of the tip of the compliant carbon fiber, the indentation test can be applied by pushing it against the myocyte horizontally (Nishimura et al., 2006b). Shear strain can be also applied by shifting the glass flake connected to a piezoelectric translator via the carbon fiber in both the longitudinal and transverse plane (Nishimura et al., 2006b).

2.2. Fluorescent voltage measurement in single cardiomyocytes

The influence of mechanical stretch on the membrane potential is one of the major fields of MEC research. We coupled the carbon-fiber technique with fluorescent voltage measurement using a transmembrane voltage-sensitive dye, which allows us to avoid the motion contamination often detected in standard patch-pipette voltage recording. Voltage-sensitive dyes can be used to monitor fast events such as action potentials and membrane depolarization, and ratiometric evaluation of two simultaneously detected emission wavelengths can effectively remove motion artifacts often detected by the standard patch-pipette technique (Knisley et al., 2000; Tai et al., 2004). However, voltage-sensitive dyes have some weaknesses. First, because voltage-sensitive dyes only provide a measurement of relative voltage change, the fluorescent signal should be calibrated against the direct electrode measurement. Second, since phototoxicity of the dye to cardiomyocytes is not negligible under high-dose (30–60 μM), it should be prevented by limiting the loading dose of the dye, reducing the illumination wattage and adding a combination of antioxidants (catalase, glucose oxidase and Trolox C) (Bullen and Saggau, 1999; Schaffer et al., 1994). We used di-8-ANEPPS, a ratiometric dye, with its emission spectrum shifting reversibly to shorter wavelengths in response to membrane depolarization (Fig. 1A). The emitted light for shorter wavelengths (560 nm) increases simultaneously with the decrease in the emitted light for longer wavelength (620 nm) during depolarization. Hence, the ratiometry of these two wavelengths theoretically cancels out the changes in fluorescence intensity caused by motion. A diagram of our experimental system is shown in Fig. 1B. After excitation of the dye at 488 nm with a filtered mercury light, the emission light (>550 nm) was separated by a dichroic beam-splitter (570 nm), filtered (560 and 620 nm, respectively) and then detected separately by photomultipliers. The ratio of the fluorescence intensities (R560/R620; fluorescence at 560 nm relative to that at 620 nm) was calculated and converted into membrane potential. The sarcomere striations of the myocytes can be simultaneously measured by bright illumination above 650 nm (Fig. 1B). Fig. 1C shows sarcomere shortening and di-8-ANEPPS fluorescence signals at 620 and 560 nm. Although motion artifacts were apparent in the 620- and 560-nm traces, the ratiometry (R560/R620) successfully cleared the artifact (Nishimura et al., 2006a).

2.3. Membrane potential response to cardiomyocyte stretching

When transient stretches were applied to quiescent rat ventricular myocytes, transient depolarization of the membrane potential was observed. Fig. 2 shows the membrane potentials (R560/R620) together with the applied stretches quantified by the relative change in the sarcomere length (Nishimura et al., 2006a). The amplitude of the depolarization increased as the stretch magnitude was increased (Fig. 2A). When the stretch ratio exceeded 15%, action potentials were invoked in some myocytes (Fig. 2A). Administration of 10 μM gadolinium, a non-specific SAC blocker, almost completely suppressed these responses (Fig. 2B). These observations were in agreement with the predictions from computational models in which SAC activity is incorporated (Kohl et al., 1998; Rice et al., 1998; Riemer et al., 1998).

Thus, our methodology combining carbon-fiber technique with fluorescent voltage measurement enables the recording of acute changes in membrane potentials in cardiomyocytes during dynamic axial stretching. Compared with our technique, other reported techniques combining membrane potential or current measurement with axial stretching allow static or relatively slow stretches (Kamkin et al., 2000; Riemer and Tung, 2003; Zeng et al., 2000). The data presented with our current technique demonstrate that the membrane potential responds to stretch in a length-dependent manner, which was most likely dependent on SAC activation.

3. Myocardial tissue study

The impact of the mechanical stretch on cardiac electrical activity has been also studied at the ventricular level by applying balloon dilatations to the left ventricles (Franz et al., 1989, 1992; Hansen et al., 1991; Hansen et al., 1990; Lerman et al., 1985; Parker et al., 2004, 2001; Zabel et al., 1996). These studies have clarified the influence of volume pulse intensity, timing, and speed on monophasic action potentials. However, it is difficult to assess the link between volume/pressure loading stresses and the stretch levels of individual cardiomyocytes because of the complex structure of the intact ventricles. In this respect, the use of excised ventricular myocardial tissue specimens is suitable for comparisons between a global stretch (corresponding to ventricular volume pulse) with local strain (corresponding to cardiomyocyte stretch), thereby facilitating the understanding of the link between them. In this section, we introduce our studies with ventricular myocardial tissue in which we performed dynamic stretching and measured electrical activity with the optical mapping technique.

3.1. Stretching device for ventricular myocardial tissue

The use of rectangular myocardial specimens has a number of advantages for studying MEC and related arrhythmias. For example, this shape enables us to visualize two-dimensional myocardial electrophysiological activity to establish the basis of arrhythmias. Furthermore, the local strain pattern in the surface can be related to a global stretch applied to the specimen. Indeed, a number of studies of MEC have been conducted with cell cultured myocardial sheets (Kong et al., 2005; Thompson et al., 2011; Zhang et al., 2008), which provides an *in vitro* preparation that can be examined under controlled conditions. However, these models rule out the role of heterogeneous structure of the real ventricular wall, which is believed to be critical for establishing a link between the cellular MEC and arrhythmias observed at the organ level. Another disadvantage of cell culture models is that when cells are grown on a rigid surface, they cannot be stretched.

In this respect, we chose to use rectangular myocardial tissue prepared from the right ventricular (RV) free wall, thus preserving its heterogeneous structure, to assess local strain (Fig. 3A) (Seo et al., 2010). To avoid tissue ischemia, the coronary artery perfusing the RV free wall was kept intact and the aorta was connected to the Langendorff apparatus for retrograde perfusion. Cyanoacrylate tissue adhesive (Vetbond™; 3M, St. Paul, MN, USA), which is often used for sealing surgical incisions of animals, was used to glue the tissue-to-tissue supports. For our purpose, we apply a transient stretch within 200 ms. Accordingly, we chose a vibration shaker (ET-126A; Labworks Inc., Costa Mesa, CA, USA), designed for general purpose vibration testing, for applying stretch. This shaker provides a large displacement capability and high acceleration with little or no velocity restrictions, and is able to move against large loads. This shaker is equipped with a displacement transducer (IW12; TWK-Elektronik, Düsseldorf, Germany) to measure the actual displacement in response to the stretches for feed-back controls. Zirconia beads (diameter, 0.5 mm) were attached to the myocardial surface (Fig. 3A) as landmarks for motion tracking, which are used for both strain measurement and optical mapping.

3.2. Optical voltage/strain mapping in myocardial tissue

Optical mapping allows the simultaneous measurement of action potentials from a large number of recording sites with a higher spatiotemporal resolution than electrical mapping with multi-electrode arrays (Sahakian et al., 2001; Schuessler et al., 1993), and

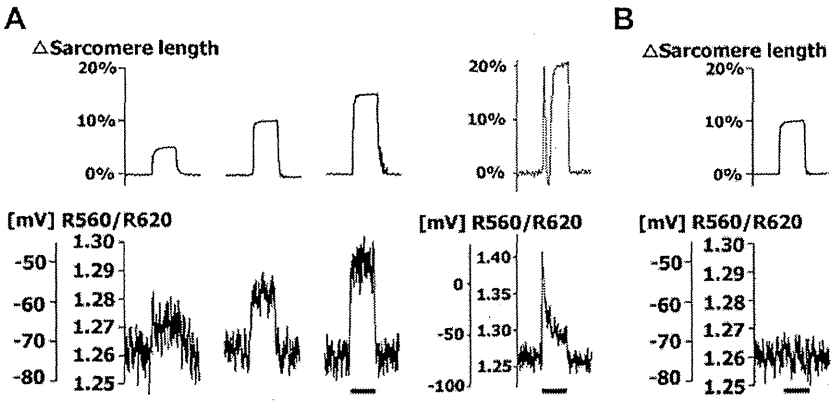

Fig. 2. Effect of dynamic stretching on resting membrane potential. A) Stretches of varying amplitudes (5%, 10%, 15%, and 20% in sarcomere length; upper traces) and the corresponding membrane potential responses (R560/R620; lower traces). Bar 500 ms. B) Effect of gadolinium (10 μM) on the resting membrane potential responses induced by dynamic stretching. Scale bar: 500 ms. The spike and notch in the sarcomere length for the 20% stretch was due to the momentary loss of length control caused by cell contraction.

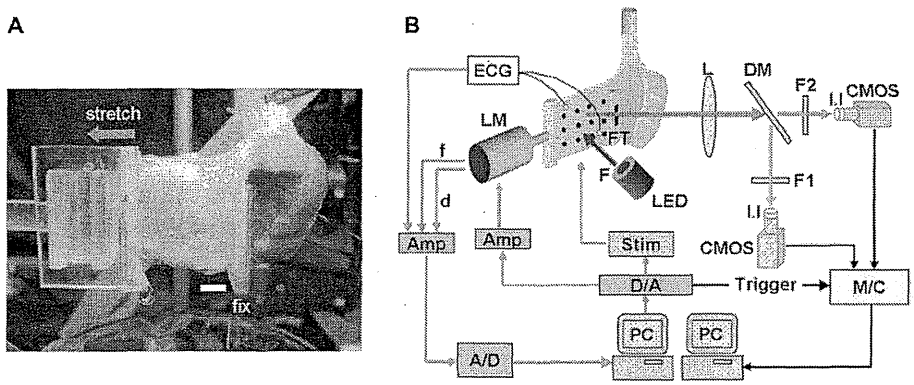

Fig. 3. Tissue preparation and the experimental setup. A) Photograph of the tissue preparation. Scale bar: 5 mm. B) Diagram of the experimental setup for tissue study. The trimmed RV wall was glued to a pair of tissue supports connected to a force transducer (FT) and a linear motor (LM). ECG, force (f) and displacement (d) signals are amplified (Amp) and recorded by a personal computer (PC) through an AD converter (A/D). Stretch and electrical stimulation commands are generated by the PC and transferred to LM and an electrical stimulator (Stim) through a DA converter (D/A). For optical voltage mapping, the tissue is illuminated by light emission diodes (LEDs). The emission light is split by a dichroic mirror (DM) and narrowed down to two frequency bands by appropriate filters (F1: 540 ± 20 nm and F2: 680 ± 20 nm). The optical images are captured by two independent CMOS cameras coupled with image intensifiers (I.I) and stored in a memory controller (M/C) and the PC. L: lens.

can be used to generate maps of electrical propagation. There also exist a number of modalities for evaluation of local strain distributions, including sonomicrometry (Toyoda et al., 2004; Villarreal et al., 1988) and tagged MRI (Moore et al., 2000; Prinzen et al., 1999). However, despite the close interdependence between electrophysiological activity and strain (i.e., MEC), there are few studies that combine multisite electrical recordings with simultaneous mechanical measurement.

We employed a marker-tracking scheme together with optical mapping to establish the relationship between strain distributions and electrical activity in cardiac preparations (Seo et al., 2010). The diagram of the experimental system is shown in Fig. 3B. The tissues were loaded with a voltage-sensitive dye, di-4-ANEPPS. Di-4-ANEPPS is known to respond to changes in the membrane potential fairly quickly and sensitively (Fluhler et al., 1985; Knisley et al., 2000), while di-8-ANEPPS, which we used in the cardiomyocyte study, has improved photostability and less phototoxicity (Bullen and Saggau, 1999; Schaffer et al., 1994). The epicardial surface of the tissues was illuminated by filtered excitation light (480 ± 10 nm) obtained from bluish-green light-emitting diodes (Nichia Chemical Industries, Tokushima, Japan), and the emitted fluorescent light was collected by a high numerical aperture complex photographic lens (50 mm F/1.2; Nikon, Tokyo, Japan), which was split by a dichroic mirror (580 nm; Andover, Salem, NH, USA) and narrowed down to two frequency bands (540 ± 20 nm and 680 ± 20 nm) through bandpass filters (Andover, Salem, NH, USA). We used two independent complementary metal oxide semiconductor (CMOS) cameras with image intensifiers (FASTCAM-Ultima; Photron, Tokyo, Japan) to simultaneously collect the dual-wavelength lights at high frame rate (500 frames/s). Conventional CMOS sensors offer advantages by achieving a very fast frame rate with a large field of view, but smaller dynamic ranges, compared with electron multiplying charge-coupled devices (EM-CCDs). On the other hand, the recent advance of scientific CMOS (sCMOS) sensors offers wide dynamic range and extremely low noise, possibly becoming major instruments for optical mapping studies (Efimov and Salama, 2012).

The optical images captured by this system have black dots arranged in a square lattice reflecting the zirconia beads attached to the tissue surface. These positional data were used for calculating epicardial local strain by dividing the distances between the bead markers in the stretched state by the corresponding distances in the reference state. This enables us to obtain local strain maps of the stretched tissue with corresponding optical maps. As noted, these positional data are also used for the motion tracking technique to remove motion-induced contamination from the optical maps.

3.3. Image processing to remove motion artifact

Motion artifact becomes more serious in tissue preparations, which disturbs the fluorescent signal along the light path and in the *x*-*y* plane. To avoid this issue, most optical mapping studies have only dealt with immobile preparations where the motion was inhibited mechanically and/or pharmacologically (e.g., butanedione monoxime and blebbistatin) (Herron et al., 2012; Lou et al., 2012). However, such preparations are nonphysiological as they ignore the role of MEC. One alternative methodological solution is to use an optical recording system based on a fiber optic image conduit, which permits the elimination of motion artifacts in myocardial tissue (Rohr and Kucera, 1998), although the number of the recording site is limited. By contrast, we have used ratiometry combined with a motion-tracking technique to resolve the problem in optical mapping (Inagaki et al., 2004; Seo et al., 2010). For motion tracking, the initial images were used as a reference, and the corresponding positions of the bead landmarks attached to the tissue surface in the successive image were automatically determined by template matching of the image of each bead. We used the positional data to determine the affine transformation matrices for the geometric distortion during the stretch or contraction. With the affine transformation based on motion tracking, we traced the tissue points, presumably a cluster of specific myocytes, during a stretch, and showed the sequential changes in the transmembrane potential of each tissue segment. Throughout the course of calculations, ratiometry with numerator wavelengths of 540 ± 20 nm and denominator wavelengths of 680 ± 20 nm was used to remove the artifacts caused by motion along the light path.

To compensate for motion artifact, other researchers have also used affine transformation (Rohde et al., 2005; Svrcek et al., 2009) or non-linear transformation (Westergaard et al., 2008). Another reported method involves the use of grid points surrounded by a constant control area in each frame to find best matches with those of the reference frame (Bagwe et al., 2005). The major difference between these techniques and ours is the use of landmarks for motion tracking, which enables more stable tracking. In fact, the images without landmarks are often devoid of distinct features, which makes it difficult to track the motion especially in the dynamically stretched tissue. The use of landmarks also facilitates

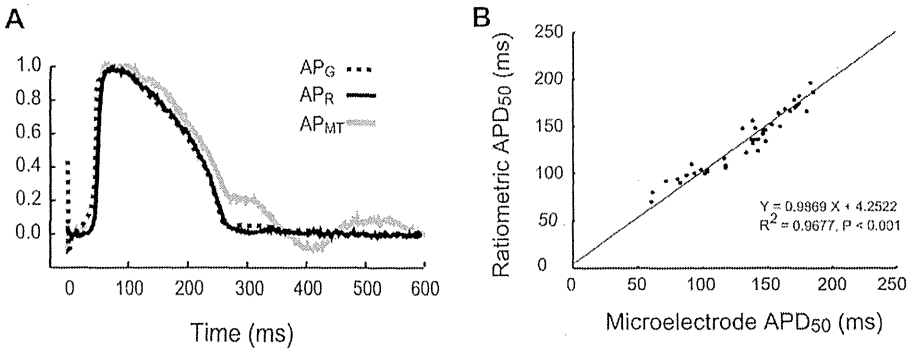

Fig. 4. Optical membrane potentials after motion tracking and/or ratiometric processing. A) Intracellular glass microelectrode signal (AP_G), ratiometric signal (AP_R), and 540 ± 20 nm wavelength signal after motion tracking (AP_{MT}). B) Scatter plot of action potential duration at 50% repolarization (APD_{50}) obtained from ratiometric and simultaneous microelectrode recordings ($n = 7$).

the quantification of epicardial strain distribution. Bourgeois and colleagues recently developed a similar but sophisticated technique in which ring-shaped markers were used for motion tracking to successfully remove motion artifact generated by heart contraction (Bourgeois et al., 2011).

Fig. 4A shows typical action potential recordings (540 ± 20 nm wavelength signal after motion tracking processing, and the ratiometric signal) from the optical mapping system, and a simultaneous recording from an intracellular glass microelectrode in the freely beating rabbit ventricle (Inagaki et al., 2004). In both optical signals after the motion tracking, the action potentials upstroke is not contaminated by motion. However, in the 540 ± 20 nm wavelength signal, the action potential plateau and repolarization remain distorted by the motion artifact. We found that ratiometry removed this artifact and gave a similar action potential contour to that obtained from a microelectrode signal. The combined results shown in Fig. 4B indicate agreement of action potential duration at 50% repolarization measured ratiometrically with that measured from microelectrode signals.

3.4. Stretch-induced excitation in myocardial tissue

The use of this technique in a tissue preparation provided us with a unique opportunity to elucidate the relationships among

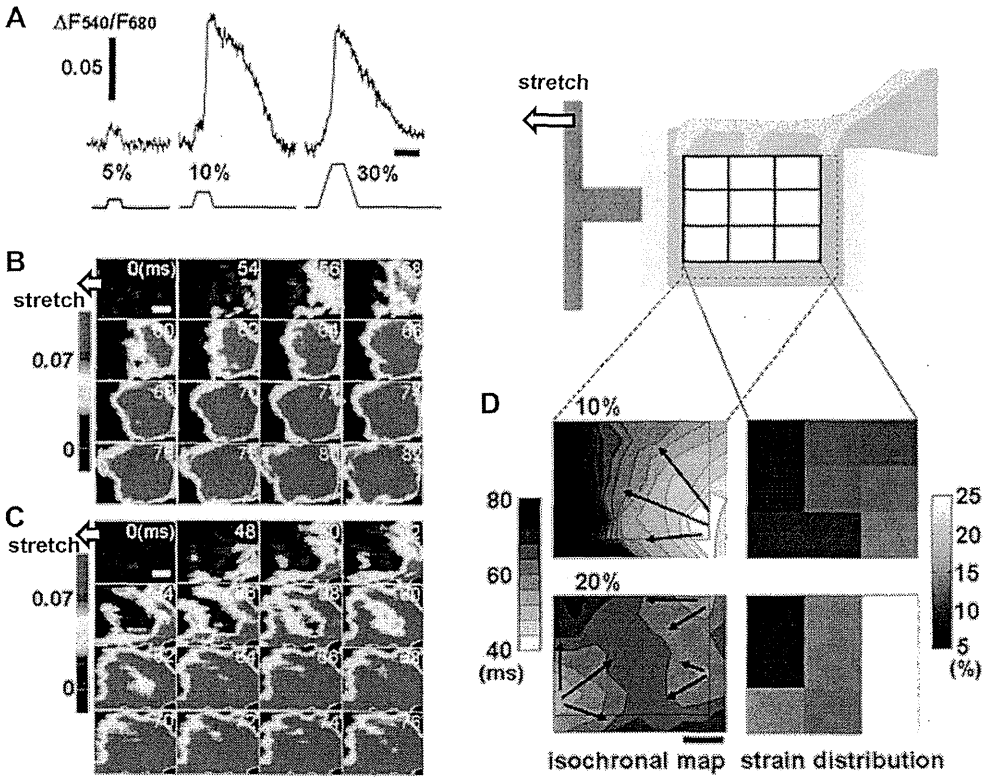

Fig. 5. Alterations in the electrical activation and strain distributions in cardiac tissues in response to stretches. A) Ratiometric optical signals in response to 5%, 10%, and 30% stretches. Scale bar: 100 ms. B and C) Representative optical maps in response to 10% and 30% stretches, respectively. The left side of the tissue was stretched leftward. The stretch starts at 0 ms. Scale bar: 4 mm. D) Representative isochronal maps of transmembrane potentials (left) and strain distributions (right). Top and bottom show 10% and 20% stretch, respectively. Scale bar: 4 mm.

electrical excitation, global strain, and local strain. Fig. 5A shows representative transmembrane potential signals in response to stretches of varying amplitudes (Seo et al., 2010). With a uniaxial stretch with a small amplitude (5%), the myocardial tissue was depolarized but an action potential was not invoked (Fig. 5A left). Above a certain level of amplitude (≥10%), however, focal excitation and its propagation were observed (Fig. 5A middle, Fig. 5B). A larger stretch (30%) induced multiple excitations (Fig. 5A right, Fig. 5C). Evaluation of the relevance between stretch-activated excitation and epicardial local strain revealed that although a uniaxial global stretch was applied to the preparation, excitation was usually only induced in a limited area where the local strain was high (Fig. 5D). Furthermore, this heterogeneity in the strain distribution reflected the complex structure of the ventricular wall, such that the excitation is initiated in regions where the wall is thin (Seo et al., 2010). This finding is supported by other experimental evidence showing that an increase in intraventricular volume by pulmonary arterial occlusion results in non-uniform stretch of the right ventricular wall, which is associated with different alterations in regional monophasic action potential morphology, including the initiation of early after depolarizations (Chen et al., 2004). Accordingly, with increased intraventricular stress, excitations are usually initiated from the region of largest strain (Quinn, 2014). Whereas the heterogeneous structure of the ventricles normally works for its vigorous contraction, adverse hemodynamic overloads in disease states lead to abnormalities in the ventricular shape and regional wall motion (Katz and Katz, 1989), which may sometimes evoke focal excitations from thinner areas.

4. Relevance of cellular mechano-electric coupling to stretch-induced arrhythmias

The mechanisms by which mechanical stretches can lead to fatal arrhythmias have been predominantly investigated by computer simulation (Pfeiffer et al., 2014; Quinn, 2014; Quinn and Kohl, 2011; Trayanova et al., 2011). Two-dimensional (Garny and Kohl, 2004) and three-dimensional (Li et al., 2004) models of ventricular tissue have demonstrated that mechanically induced sustained arrhythmias (i.e., re-entry) may occur only when focal excitations initiated by mechanical stimuli interact with the preceding electrical activation of the myocardial tissue. Our experimental results suggest that the focal excitation can be induced with intermediate-strength mechanical stimuli. To elucidate the link between the focal ectopic excitation and a fatal arrhythmia, detailed evaluation of spatio-temporal electrical behavior is necessary. Therefore, we investigated the characteristics of mechanically-induced ectopy in the whole heart and its potential for inducing sustained fatal arrhythmias with our modified optical mapping system (Fig. 6A) coupled with the motion tracking and the image processing techniques introduced in the tissue study. We applied a controlled volume pulse to the isolated Langendorff-perfused rabbit RV at various coupling intervals (90–130 ms) with a preceding electrical stimulus (Seo et al., 2010). As shown in Fig. 6B, we observed re-entrant arrhythmias with a volume pulse of intermediate size (1.5 mL). As shown in Fig. 6C, a large volume pulse (2 mL) did not elicit arrhythmias. Importantly, only an intermediate volume pulse (1.5 mL) applied after a proper coupling interval (110 ms) triggered re-entrant arrhythmias.

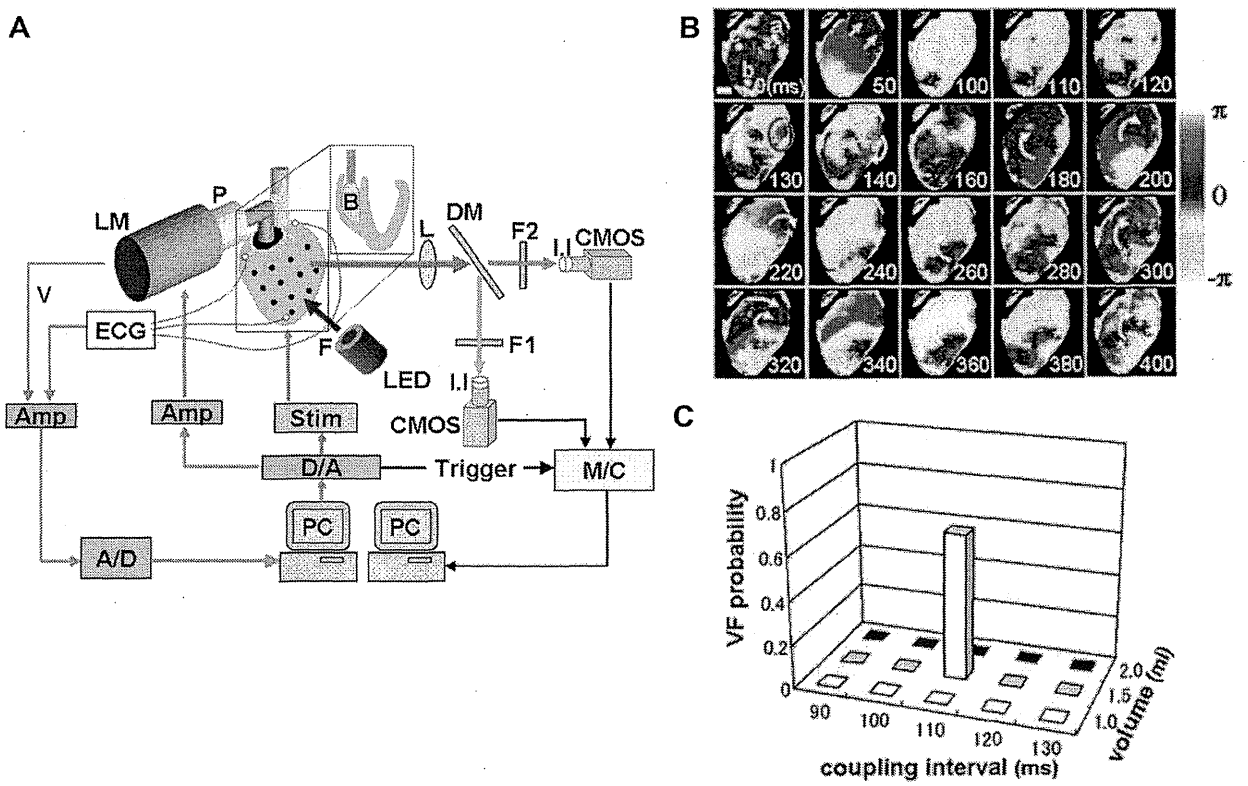

Fig. 6. Occurrence of stretch-induced re-entrant arrhythmias in the whole heart preparations. A) Diagram of the experimental setup for whole heart study. This system is a modified version of the tissue stretching system described in Fig. 3B. A balloon (B) is inserted into RV of the perfused whole heart and is connected to a piston pump (P) with a linear motor (LM) to apply servo-controlled volume pulses. B) Representative phase maps of re-entrant arrhythmia. The volume pulse (1.5 mL) was applied at 110 ms after an electrical stimulus started at 0 ms. Scale bar: 4 mm *Phase singularity points. C) Excitation probabilities in relation to the coupling intervals and the intensities of the volume pulses ($n = 3$).

There are extensive studies examining the electrophysiological effects of volume increases in the intact heart (Franz et al., 1989, 1992; Hansen et al., 1991; Hansen et al., 1990; Parker et al., 2004, 2001; Zabel et al., 1996). For example, Hansen et al. examined the effects of rapid, transient, volume increases in an isolated, perfused, canine ventricle, and observed ectopic excitations during or shortly after the volume pulse, although they did not record direct electrophysiological behavior (Hansen et al., 1990). Franz et al. also investigated the effects of increases in ventricular diastolic volume on epicardial monophasic action potentials in Langendorff perfused rabbit hearts, and clearly demonstrated its effect on the incidence of extrasystole (Franz et al., 1992). However, no experimental studies have succeeded in determining the characteristics of stretch-induced fatal arrhythmias with this preparation. Recent advances in optical mapping and its combination with our motion-tracking technique provide the first evidence that the re-entrant arrhythmias can be induced by intermediate-volume pulse coupled with preceding electrical stimulation (Fig. 6B) (Seo et al., 2010). One of the limitations in our system is that the mapped region in the intact heart is restricted to the field of view of the sensor, which makes it difficult to track electrical waves as they can drift in and out of view. To overcome this problem, novel techniques to image the entire surface (front and back) of the heart such as panoramic imaging are needed (Bourgeois et al., 2012; Kay et al., 2006).

Our proposed mechanism of how cellular MEC leads to fatal arrhythmias observed in the whole heart preparation is shown in Fig. 7. First, membrane potential responds to stretch in an amplitude-dependent manner in single cardiomyocytes (Fig. 2). At the tissue level, conversely, the electrical activity is highly heterogeneous especially when the intermediate strength of global stretch is applied to the tissue (Fig. 5). This is because of the modulation by the inhomogeneous structure of the ventricular wall. At the organ level, when the medium volume pulse is applied at a certain coupling interval, the stretch-induced focal excitation can develop into fatal re-entrant arrhythmias (Fig. 6). This scenario may explain the etiology of *commotio cordis*, which often occurs because of a nonpenetrating chest wall blow when the rib, sternum, and heart are themselves uninjured. Indeed, experimentally, *commotio cordis* was reported to be induced by baseball projectiles with intermediate strength (Link et al., 2003), although the mechanisms have been elusive. Our studies indicate the non-uniformity of the ventricular wall structure is associated with a high susceptibility to fatal arrhythmias, which may be a predictor of sudden cardiac death.

5. Future directions: laser optical trap combined with real-time Ca^{2+} imaging in cardiomyocytes

In this review, we have described our observations of mechanical stress-induced electrical activities made at cell, tissue, and organ levels, and discussed their inter-relationships. However, to gain further insight into the mechanisms underlying mechanical stress-induced electrical activity, we need to extend our limit of observation to the subcellular level. As the first step toward this goal, we made a preliminary attempt to determine how cardiomyocytes respond to a minute stimulus applied to the sarcolemma. As an actuator to apply a stimulus of small magnitude, we adopted the laser optical trap technique (Sugiura et al., 1998) with which we can trap and manipulate a small bead under a microscope (IX70; Olympus, Tokyo, Japan) using an infrared laser beam (1064 nm IRCL-1W; CrystaLaser, Reno, NV, USA) introduced via an objective lens (60×, n.a. 1.4). Cardiomyocytes isolated from 6-week-old Wistar rats were loaded with calcium indicator (Fluo-8) and fixed on laminin-coated coverslips in buffer containing 1.1 mM Ca^{2+}. To this preparation we added a small bead (diameter 6.0 μm Polybead Carboxylated; Polysciences Inc., Warrington, PA, USA) coated with an RGD peptide (Sigma–Aldrich, St. Louis MO, USA) as the selective ligand to integrin. We selected a bead firmly attached to the sarcolemma, and then trapped and moved it with the optical trap

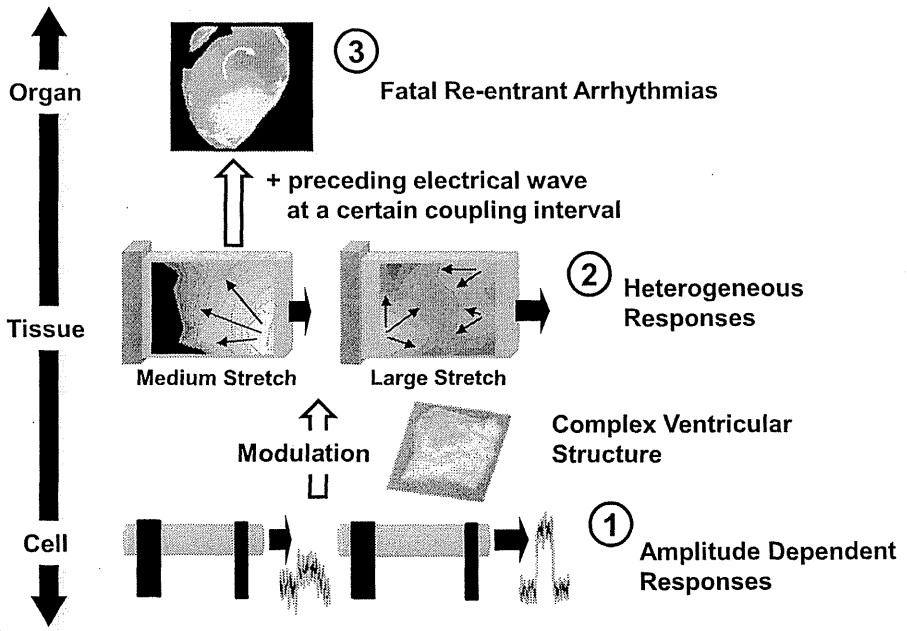

Fig. 7. Schematic illustration of our proposed mechanism. (1) At the cellular level, membrane potential responds to stretch in an amplitude-dependent manner. (2) At the tissue level, however, globally applied stretch is modulated by the inhomogeneous structure of the ventricular wall to cause heterogeneous excitation. (3) This effect becomes manifest in response to stretch of medium intensity and may trigger fatal arrhythmias when coupled with a preceding electrical propagation.

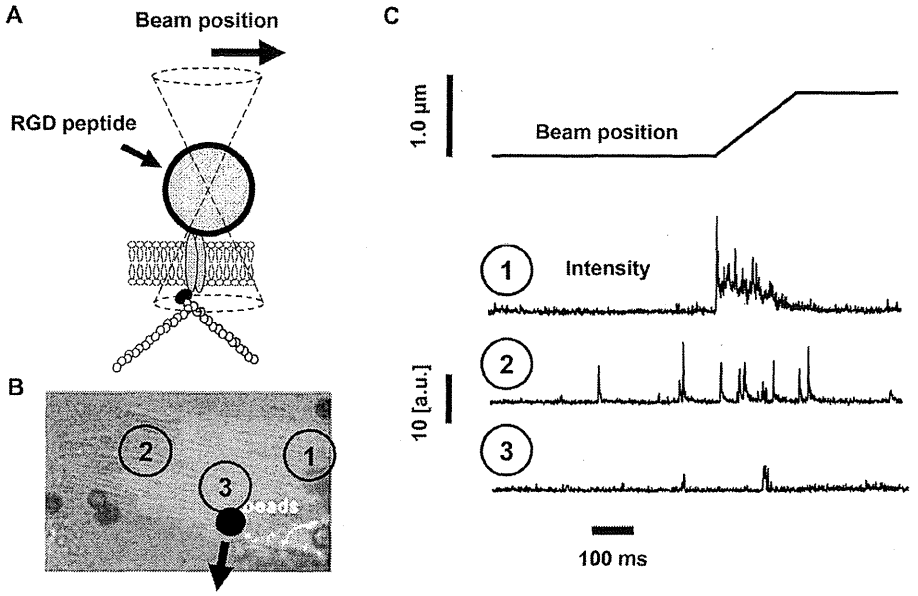

Fig. 8. Ca^{2+} spark responses to subcellular level stimulus. A) A microsphere coated with RGD peptide was attached to the sarcolemma and trapped by the laser optical trap. Stimulus of small amplitude was applied by moving the laser beam. B) The microsphere was moved in the transverse direction (arrow) and the fluorescent signals were sampled at three locations in the same cell. C) Top row: displacement of the laser beam. 2nd to 4th rows: fluorescent signals from the Ca^{2+} indicator at 3 locations indicated in B. Ca^{2+} sparks coincided with the mechanical stimulus were observed in the locations remote from the stimulus site (1 and 2).

linearly with a small amplitude (<1 μm) by steering the galvano-mirror equipped in the beam path (Fig. 8A). Fluorescent images were viewed and recorded by spinning disc confocal laser scanning microscope (CSU-X1; Yokogawa, Tokyo, Japan) with a high-speed camera (SV-200i; Photoron, Tokyo, Japan). The detailed method is described in the online supplementary material.

The applied stimulus provoked calcium sparks, but they were clustered in a remote area rather than at the site of the stimulus (Fig. 8B and C). Furthermore, treatment with colchicine, which inhibits microtubule polymerization, abolished these responses (data not shown). Although the number of observations is limited, these data suggest a role of the cytoskeletal network in the transmission of a mechanical stimulus within the myocyte, consistent with earlier reports (Iribe et al., 2009; Prosser et al., 2011). This may be related to the observation by Parker that treatment with taxol, which polymerizes microtubules, increased the frequency of arrhythmias induced by volume pulse to the rabbit left ventricles (Parker et al., 2001). By contrast, in a swine model of *commotio cordis*, colchicine treatment increased the probability of chest impact-induced ventricular fibrillation (Madias et al., 2008).

It has been demonstrated that Ca^{2+} waves can be initiated in damaged myocardial region where non-uniform muscle are subjected to contraction-associated stretch, which may lead to premature beats and triggered arrhythmias (ter Keurs, 2012; Wakayama et al., 2005). Such a non-uniform activity in myocardium is often observed in pathological state such as myocardial infarction and heart failure (Quinn, 2014). It is evident that acute stretch of ventricles can result in re-entrant arrhythmias by triggering through stretch-induced changes in membrane potential (Seo et al., 2010), although intracellular Ca^{2+} handling may play other roles especially in diseases. Although further studies are needed, continuing studies at multiple biological system levels and possible integration by numerical simulation will help further our understanding of mechanical stress-induced arrhythmia and to develop effective preventative measures.

6. Conclusions

In this review, we introduced our unique experimental techniques in various experimental settings. Our studies provide a possible scenario for the link between cardiomyocyte MEC and fatal arrhythmias induced by acute mechanical stresses. Further development and utility of these techniques will promote basic studies and a comprehensive understanding of the molecular mechanisms of MEC and its translation to stretch-induced arrhythmias.

Editors' note

Please see also related communications in this issue by Yu et al. (2014) and Wang et al. (2014).

Acknowledgments

This research is supported by the Japan Society for the Promotion of Science (JSPS) through its "Funding Program for World-Leading Innovative R&D on Science and Technology (FIRST Program)" and the JSPS Postdoctoral Fellowship for Research Abroad to K. S.. Figs. 1 and 2 were reprinted from Cardiovascular Research 72, Nishimura, S., Kawai, Y., Nakajima, T., Hosoya, Y., Fujita, H., Katoh, M., Yamashita, H., Nagai, R., Sugiura, S., Membrane potential of rat ventricular myocytes responds to axial stretch in phase, amplitude and speed-dependent manners, pp. 403–411, 2006, with permission from Oxford University Press. Figs. 3, 5 and 6 were reprinted from Circulation Research 106, Seo, K., Inagaki, M., Nishimura, S., Hidaka, I., Sugimachi, M., Hisada, T., Sugiura, S., Structural Heterogeneity in the Ventricular Wall Plays a Significant Role in the Initiation of Stretch-Induced Arrhythmias in Perfused Rabbit Right Ventricular Tissues and Whole Heart Preparations, pp. 176–184, 2010, with permission from Wolters Kluwer Health. Fig. 4 was reprinted from Proceedings of the 26th Annual International Conference of the IEEE EMBS, Inagaki, M., Hidaka, I., Aiba, T., Tatewaki, T., Sunagawa, K., Sugimachi, M., High resolution optical mapping of

cardiac action potentials in freely beating rabbit hearts, pp. 3578–3580, 2004, with permission from IEEE.

References

Aimond, F., Alvarez, J.L., Rauzier, J.M., Lorente, P., Vassort, G., 1999. Ionic basis of ventricular arrhythmias in remodeled rat heart during long-term myocardial infarction. Cardiovasc. Res. 42, 402–415.

Allen, D.G., Kentish, J.C., 1988. Calcium concentration in the myoplasm of skinned ferret ventricular muscle following changes in muscle length. J. Physiol. 407, 489–503.

Bagwe, S., Berenfeld, O., Vaidya, D., Morley, G.E., Jalife, J., 2005. Altered right atrial excitation and propagation in connexin40 knockout mice. Circulation 112, 2245–2253.

Belus, A., White, E., 2003. Streptomycin and intracellular calcium modulate the response of single guinea-pig ventricular myocytes to axial stretch. J. Physiol. 546, 501–509.

Bett, G.C., Sachs, F., 2000. Whole-cell mechanosensitive currents in rat ventricular myocytes activated by direct stimulation. J. Membr. Biol. 173, 255–263.

Bourgeois, E.B., Bachtel, A.D., Huang, J., Walcott, G.P., Rogers, J.M., 2011. Simultaneous optical mapping of transmembrane potential and wall motion in isolated, perfused whole hearts. J. Biomed. Opt. 16, 096020.

Bourgeois, E.B., Reeves, H.D., Walcott, G.P., Rogers, J.M., 2012. Panoramic optical mapping shows wavebreak at a consistent anatomical site at the onset of ventricular fibrillation. Cardiovasc. Res. 93, 272–279.

Bullen, A., Saggau, P., 1999. High-speed, random-access fluorescence microscopy: II. Fast quantitative measurements with voltage-sensitive dyes. Biophys. J. 76, 2272–2287.

Calaghan, S., White, E., 2004. Activation of Na+-H+ exchange and stretch-activated channels underlies the slow inotropic response to stretch in myocytes and muscle from the rat heart. J. Physiol. 559, 205–214.

Chen, R.L., Penny, D.J., Greve, G., Lab, M.J., 2004. Stretch-induced regional mechanoelectric dispersion and arrhythmia in the right ventricle of anesthetized lambs. Am. J. Physiol. Heart Circ. Physiol. 286, H1008–H1014.

Craelius, W., Chen, V., el-Sherif, N., 1988. Stretch activated ion channels in ventricular myocytes. Biosci. Rep. 8, 407–414.

Efimov, I., Salama, G., 2012. The future of optical mapping is bright: RE: review on: "Optical Imaging of Voltage and Calcium in Cardiac Cells and Tissues" by Herron, Lee, and Jalife. Circ. Res. 110, e70-1.

Efimov, I.R., Nikolski, V.P., Salama, G., 2004. Optical imaging of the heart. Circ. Res. 95, 21–33.

Fasciano 2nd, R.W., Tung, L., 1999. Factors governing mechanical stimulation in frog hearts. Am. J. Physiol. 277, H2311–H2320.

Flubler, E., Burnham, V.G., Loew, L.M., 1985. Spectra, membrane binding, and potentiometric responses of new charge shift probes. Biochemistry 24, 5749–5755.

Franz, M.R., Burkhoff, D., Yue, D.T., Sagawa, K., 1989. Mechanically induced action potential changes and arrhythmia in isolated and in situ canine hearts. Cardiovasc Res. 23, 213–223.

Franz, M.R., Cima, R., Wang, D., Profitt, D., Kurz, R., 1992. Electrophysiological effects of myocardial stretch and mechanical determinants of stretch-activated arrhythmias. Circulation 86, 968–978.

Fujiwara, K., Tanaka, H., Mani, H., Nakagami, T., Takamatsu, T., 2008. Burst emergence of intracellular Ca2+ waves evokes arrhythmogenic oscillatory depolarization via the Na+-Ca2+ exchanger: simultaneous confocal recording of membrane potential and intracellular Ca2+ in the heart. Circ. Res. 103, 509–518.

Gannier, F., White, E., Lacampagne, A., Garnier, D., Le Guennec, J.Y., 1994. Streptomycin reverses a large stretch induced increases in [Ca2+]i in isolated guinea pig ventricular myocytes. Cardiovasc. Res. 28, 1193–1198.

Garnier, D., 1994. Attachment procedures for mechanical manipulation of isolated cardiac myocytes: a challenge. Cardiovasc. Res. 28, 1758–1764.

Garny, A., Kohl, P., 2004. Mechanical induction of arrhythmias during ventricular repolarization: modeling cellular mechanisms and their interaction in two dimensions. Ann. N. Y. Acad. Sci. 1015, 133–143.

Hansen, D.E., Borganelli, M., Stacy Jr., G.P., Taylor, L.K., 1991. Dose-dependent inhibition of stretch-induced arrhythmias by gadolinium in isolated canine ventricles. Evidence for a unique mode of antiarrhythmic action. Circ. Res. 69, 820–831.

Hansen, D.E., Craig, C.S., Hondeghem, L.M., 1990. Stretch-induced arrhythmias in the isolated canine ventricle. Evidence for the importance of mechanoelectrical feedback. Circulation 81, 1094–1105.

Herron, T.J., Lee, P., Jalife, J., 2012. Optical imaging of voltage and calcium in cardiac cells & tissues. Circ. Res. 110, 609–623.

Inagaki, M., Hidaka, I., Aiba, T., Tatewaki, T., Sunagawa, K., Sugimachi, M., 2004. High resolution optical mapping of cardiac action potentials in freely beating rabbit hearts. Conf. Proc. IEEE Eng. Med. Biol. Soc. 5, 3578–3580.

Iribe, G., Helmes, M., Kohl, P., 2007. Force-length relations in isolated intact cardiomyocytes subjected to dynamic changes in mechanical load. Am. J. Physiol. Heart Circ. Physiol. 292, H1487–H1497.

Iribe, G., Jin, H., Kaihara, K., Naruse, K., 2010. Effects of axial stretch on sarcolemmal BKCa channels in post-hatch chick ventricular myocytes. Exp. Physiol. 95, 699–711.

Iribe, G., Ward, C.W., Camelliti, P., Bollensdorff, C., Mason, F., Burton, R.A., Garny, A., Morphew, M.K., Hoenger, A., Lederer, W.J., Kohl, P., 2009. Axial stretch of rat single ventricular cardiomyocytes causes an acute and transient increase in Ca2+ spark rate. Circ. Res. 104, 787–795.

Janse, M.J., 2004. Electrophysiological changes in heart failure and their relationship to arrhythmogenesis. Cardiovasc. Res. 61, 208–217.

Jian, Z., Han, H., Zhang, T., Puglisi, J., Izu, L.T., Shaw, J.A., Onofiok, E., Erickson, J.R., Chen, Y.J., Horvath, B., Shimkunas, R., Xiao, W., Li, Y., Pan, T., Chan, J., Banyasz, T., Tardiff, J.C., Chiamvimonvat, N., Bers, D.M., Lam, K.S., Chen-Izu, Y., 2014. Mechanochemotransduction during cardiomyocyte contraction is mediated by localized nitric oxide signaling. Sci. Signal 7, ra27.

Kamkin, A., Kiseleva, I., Isenberg, G., 2000. Stretch-activated currents in ventricular myocytes: amplitude and arrhythmogenic effects increase with hypertrophy. Cardiovasc. Res. 48, 409–420.

Kamkin, A., Kiseleva, I., Isenberg, G., 2003. Ion selectivity of stretch-activated cation currents in mouse ventricular myocytes. Pflugers Arch. 446, 220–231.

Katz, A.M., Katz, P.B., 1989. Homogeneity out of heterogeneity. Circulation 79, 712–717.

Kay, M.W., Walcott, G.P., Gladden, J.D., Melnick, S.B., Rogers, J.M., 2006. Lifetimes of epicardial rotors in panoramic optical maps of fibrillating swine ventricles. Am. J. Physiol. Heart Circ. Physiol. 291, H1935–H1941.

Khairallah, R.J., Shi, G., Sbrana, F., Prosser, B.L., Borroto, C., Mazaitis, M.J., Hoffman, E.P., Mahurkar, A., Sachs, F., Sun, Y., Chen, Y.W., Raiteri, R., Lederer, W.J., Dorsey, S.G., Ward, C.W., 2012. Microtubules underlie dysfunction in duchenne muscular dystrophy. Sci. Signal 5, ra56.

Knisley, S.B., Justice, R.K., Kong, W., Johnson, P.L., 2000. Ratiometry of transmembrane voltage-sensitive fluorescent dye emission in hearts. Am. J. Physiol. Heart Circ. Physiol. 279, H1421–H1433.

Kohl, P., Day, K., Noble, D., 1998. Cellular mechanisms of cardiac mechano-electric feedback in a mathematical model. Can. J. Cardiol. 14, 111–119.

Kohl, P., Sachs, F., Franz, M.R., 2011. Cardiac Mechano-electric Coupling and Arrhythmias, second ed. Oxford University Press, Oxford ; New York.

Kong, C.R., Bursac, N., Tung, L., 2005. Mechanoelectrical excitation by fluid jets in monolayers of cultured cardiac myocytes. J. Appl. Physiol. (1985) 98, 2328–2336 discussion 2320.

Le Guennec, J.Y., Peineau, N., Argibay, J.A., Mongo, K.G., Garnier, D., 1990. A new method of attachment of isolated mammalian ventricular myocytes for tension recording: length dependence of passive and active tension. J. Mol. Cell. Cardiol. 22, 1083–1093.

Lerman, B.B., Burkhoff, D., Yue, D.T., Franz, M.R., Sagawa, K., 1985. Mechanoelectrical feedback: independent role of preload and contractility in modulation of canine ventricular excitability. J. Clin. Invest. 76, 1843–1850.

Li, W., Kohl, P., Trayanova, N., 2004. Induction of ventricular arrhythmias following mechanical impact: a simulation study in 3D. J. Mol. Histol. 35, 679–686.

Link, M.S., 2012. Commotio cordis: ventricular fibrillation triggered by chest impact-induced abnormalities in repolarization. Circ. Arrhythm. Electrophysiol. 5, 425–432.

Link, M.S., Maron, B.J., Wang, P.J., VanderBrink, B.A., Zhu, W., Estes 3rd, N.A., 2003. Upper and lower limits of vulnerability to sudden arrhythmic death with chest-wall impact (commotio cordis). J. Am. Coll. Cardiol. 41, 99–104.

Lou, Q., Li, W., Efimov, I.R., 2012. The role of dynamic instability and wavelength in arrhythmia maintenance as revealed by panoramic imaging with blebbistatin vs. 2,3-butanedione monoxime. Am. J. Physiol. Heart Circ. Physiol. 302, H262–H269.

Madias, C., Maron, B.J., Supron, S., Estes 3rd, N.A., Link, M.S., 2008. Cell membrane stretch and chest blow-induced ventricular fibrillation: commotio cordis. J. Cardiovasc Electrophysiol. 19, 1304–1309.

Moore, C.C., Lugo-Olivieri, C.H., McVeigh, E.R., Zerhouni, E.A., 2000. Three-dimensional systolic strain patterns in the normal human left ventricle: characterization with tagged MR imaging. Radiology 214, 453–466.

Nishimura, S., Kawai, Y., Nakajima, T., Hosoya, Y., Fujita, H., Katoh, M., Yamashita, H., Nagai, R., Sugiura, S., 2006a. Membrane potential of rat ventricular myocytes responds to axial stretch in phase, amplitude and speed-dependent manners. Cardiovasc. Res. 72, 403–411.

Nishimura, S., Nagai, S., Katoh, M., Yamashita, H., Saeki, Y., Okada, J., Hisada, T., Nagai, R., Sugiura, S., 2006b. Microtubules modulate the stiffness of cardiomyocytes against shear stress. Circ. Res. 98, 81–87.

Nishimura, S., Seo, K., Nagasaki, M., Hosoya, Y., Yamashita, H., Fujita, H., Nagai, R., Sugiura, S., 2008. Responses of single-ventricular myocytes to dynamic axial stretching. Prog. Biophys. Mol. Biol. 97, 282–297.

Nishimura, S., Yasuda, S., Katoh, M., Yamada, K.P., Yamashita, H., Saeki, Y., Sunagawa, K., Nagai, R., Hisada, T., Sugiura, S., 2004. Single cell mechanics of rat cardiomyocytes under isometric, unloaded, and physiologically loaded conditions. Am. J. Physiol. Heart Circ. Physiol. 287, H196–H202.

Niu, W., Sachs, F., 2003. Dynamic properties of stretch-activated K+ channels in adult rat atrial myocytes. Prog. Biophys. Mol. Biol. 82, 121–135.

Palmer, R.E., Brady, A.J., Roos, K.P., 1996. Mechanical measurements from isolated cardiac myocytes using a pipette attachment system. Am. J. Physiol. 270, C697–C704.

Parker, K.K., Lavelle, J.A., Taylor, L.K., Wang, Z., Hansen, D.E., 2004. Stretch-induced ventricular arrhythmias during acute ischemia and reperfusion. J. Appl. Physiol. (1985) 97, 377–383.

Parker, K.K., Taylor, L.K., Atkinson, J.B., Hansen, D.E., Wikswo, J.P., 2001. The effects of tubulin-binding agents on stretch-induced ventricular arrhythmias. Eur. J. Pharmacol. 417, 131–140.
Pfeiffer, E.R., Tangney, J.R., Omens, J.H., McCulloch, A.D., 2014. Biomechanics of cardiac electromechanical coupling and mechanoelectric feedback. J. Biomech. Eng. 136, 021007.
Prinzen, F.W., Hunter, W.C., Wyman, B.T., McVeigh, E.R., 1999. Mapping of regional myocardial strain and work during ventricular pacing: experimental study using magnetic resonance imaging tagging. J. Am. Coll. Cardiol. 33, 1735–1742.
Prosser, B.L., Ward, C.W., Lederer, W.J., 2011. X-ROS signaling: rapid mechano-chemo transduction in heart. Science 333, 1440–1445.
Quinn, T.A., 2014. The importance of non-uniformities in mechano-electric coupling for ventricular arrhythmias. J. Interv. Card. Electrophysiol. 39, 25–35.
Quinn, T.A., Kohl, P., 2011. Mechanical triggers and facilitators of ventricular tachyarrhythmias. In: Kohl, P., Sachs, F., Franz, M.R. (Eds.), Cardiac Mechano-electric Coupling and Arrhythmias. Oxford University Press, Oxford; New York, pp. 160–167.
Ravens, U., 2003. Mechano-electric feedback and arrhythmias. Prog. Biophys. Mol. Biol. 82, 255–266.
Rice, J.J., Winslow, R.L., Dekanski, J., McVeigh, E., 1998. Model studies of the role of mechano-sensitive currents in the generation of cardiac arrhythmias. J. Theor. Biol. 190, 295–312.
Riemer, T.L., Sobie, E.A., Tung, L., 1998. Stretch-induced changes in arrhythmogenesis and excitability in experimentally based heart cell models. Am. J. Physiol. 275, H431–H442.
Riemer, T.L., Tung, L., 2003. Stretch-induced excitation and action potential changes of single cardiac cells. Prog. Biophys. Mol. Biol. 82, 97–110.
Rohde, G.K., Dawant, B.M., Lin, S.F., 2005. Correction of motion artifact in cardiac optical mapping using image registration. IEEE Trans. Biomed. Eng. 52, 338–341.
Rohr, S., Kucera, J.P., 1998. Optical recording system based on a fiber optic image conduit: assessment of microscopic activation patterns in cardiac tissue. Biophys. J. 75, 1062–1075.
Sachs, F., 2010. Stretch-activated ion channels: what are they? Physiology (Bethesda) 25, 50–56.
Sachs, F., 2011. Stretch-activated channels in the heart. In: Kohl, P., Sachs, F., Franz, M.R. (Eds.), Cardiac Mechano-electric Coupling and Arrhythmias. Oxford University Press, Oxford ; New York, pp. 11–18.
Sahakian, A.V., Peterson, M.S., Shkurovich, S., Hamer, M., Votapka, T., Ji, T., Swiryn, S., 2001. A simultaneous multichannel monophasic action potential electrode array for in vivo epicardial repolarization mapping. IEEE Trans. Biomed. Eng. 48, 345–353.
Sasaki, N., Mitsuiye, T., Noma, A., 1992. Effects of mechanical stretch on membrane currents of single ventricular myocytes of guinea-pig heart. Jpn. J. Physiol. 42, 957–970.
Schaffer, P., Ahammer, H., Muller, W., Koidl, B., Windisch, H., 1994. Di-4-ANEPPS causes photodynamic damage to isolated cardiomyocytes. Pflugers Arch. 426, 548–551.
Schuessler, R.B., Kawamoto, T., Hand, D.E., Mitsuno, M., Bromberg, B.I., Cox, J.L., Boineau, J.P., 1993. Simultaneous epicardial and endocardial activation sequence mapping in the isolated canine right atrium. Circulation 88, 250–263.
Scimia, M.C., Hurtado, C., Ray, S., Metzler, S., Wei, K., Wang, J., Woods, C.E., Purcell, N.H., Catalucci, D., Akasaka, T., Bueno, O.F., Vlasuk, G.P., Kaliman, P., Bodmer, R., Smith, L.H., Ashley, E., Mercola, M., Brown, J.H., Ruiz-Lozano, P., 2012. APJ acts as a dual receptor in cardiac hypertrophy. Nature 488, 394–398.
Seo, K., Inagaki, M., Nishimura, S., Hidaka, I., Sugimachi, M., Hisada, T., Sugiura, S., 2010. Structural heterogeneity in the ventricular wall plays a significant role in the initiation of stretch-induced arrhythmias in perfused rabbit right ventricular tissues and whole heart preparations. Circ. Res. 106, 176–184.
Seo, K., Rainer, P.P., Lee, D.I., Hao, S., Bedja, D., Birnbaumer, L., Cingolani, O.H., Kass, D.A., 2014. Hyperactive adverse mechanical stress responses in dystrophic heart are coupled to transient receptor potential canonical 6 and blocked by cGMP-protein kinase G modulation. Circ. Res. 114, 823–832.
Sugiura, S., Kobayakawa, N., Fujita, H., Yamashita, H., Momomura, S., Chaen, S., Omata, M., Sugi, H., 1998. Comparison of unitary displacements and forces between 2 cardiac myosin isoforms by the optical trap technique: molecular basis for cardiac adaptation. Circ. Res. 82, 1029–1034.
Sugiura, S., Nishimura, S., Yasuda, S., Hosoya, Y., Katoh, K., 2006. Carbon fiber technique for the investigation of single-cell mechanics in intact cardiac myocytes. Nat. Protoc. 1, 1453–1457.
Svrcek, M., Rutherford, S., Chen, A.Y., Provaznik, I., Smaill, B., 2009. Characteristics of motion artifacts in cardiac optical mapping studies. Conf. Proc. IEEE Eng. Med. Biol. Soc. 2009, 3240–3243.
Taggart, P., Lab, M., 2008. Cardiac mechano-electric feedback and electrical restitution in humans. Prog. Biophys. Mol. Biol. 97, 452–460.
Tai, D.C., Caldwell, B.J., LeGrice, I.J., Hooks, D.A., Pullan, A.J., Smaill, B.H., 2004. Correction of motion artifact in transmembrane voltage-sensitive fluorescent dye emission in hearts. Am. J. Physiol. Heart Circ. Physiol. 287, H985–H993.
ter Keurs, H.E., 2012. The interaction of Ca2+ with sarcomeric proteins: role in function and dysfunction of the heart. Am. J. Physiol. Heart Circ. Physiol. 302, H38–H50.
ter Keurs, H.E., Shinozaki, T., Zhang, Y.M., Zhang, M.L., Wakayama, Y., Sugai, Y., Kagaya, Y., Miura, M., Boyden, P.A., Stuyvers, B.D., Landesberg, A., 2008. Sarcomere mechanics in uniform and non-uniform cardiac muscle: a link between pump function and arrhythmias. Prog. Biophys. Mol. Biol. 97, 312–331.
Thompson, S.A., Copeland, C.R., Reich, D.H., Tung, L., 2011. Mechanical coupling between myofibroblasts and cardiomyocytes slows electric conduction in fibrotic cell monolayers. Circulation 123, 2083–2093.
Tomaselli, G.F., Marban, E., 1999. Electrophysiological remodeling in hypertrophy and heart failure. Cardiovasc. Res. 42, 270–283.
Toyoda, T., Baba, H., Akasaka, T., Akiyama, M., Neishi, Y., Tomita, J., Sukmawan, R., Koyama, Y., Watanabe, N., Tamano, S., Shinomura, R., Komuro, I., Yoshida, K., 2004. Assessment of regional myocardial strain by a novel automated tracking system from digital image files. J. Am. Soc. Echocardiogr. 17, 1234–1238.
Trayanova, N.A., Gurev, V., Constantino, J., Hu, Y., 2011. Mathematical models of ventricular mechano-electric coupling and arrhythmia. In: Kohl, P., Sachs, F., Franz, M.R. (Eds.), Cardiac Mechano-electric Coupling and Arrhythmias. Oxford University Press, Oxford; New York, pp. 258–266.
Villarreal, F.J., Waldman, L.K., Lew, W.Y., 1988. Technique for measuring regional two-dimensional finite strains in canine left ventricle. Circ. Res. 62, 711–721.
Wang, K., Terrar, D., Gavaghan, D.J., Mu-u-min, R., Kohl, P., Bollensdorff, C., 2014. Living cardiac tissue slices: An organotypic pseudo two-dimensional model for cardiac biophysics research. Prog. Bio. Mol. Biol. 115 (2-3), 314–327. http://dx.doi.org/10.1016/j.pbiomolbio.2014.08.006.
Wakayama, Y., Miura, M., Stuyvers, B.D., Boyden, P.A., ter Keurs, H.E., 2005. Spatial nonuniformity of excitation-contraction coupling causes arrhythmogenic Ca2+ waves in rat cardiac muscle. Circ. Res. 96, 1266–1273.
Ward, M.L., Williams, I.A., Chu, Y., Cooper, P.J., Ju, Y.K., Allen, D.G., 2008. Stretch-activated channels in the heart: contributions to length-dependence and to cardiomyopathy. Prog. Biophys. Mol. Biol. 97, 232–249.
Westergaard, F., Umapathy, K., Masse, S., Sevaptsidis, E., Asta, J., Farid, T., Nair, K., Krishnan, S., Nanthakumar, K., 2008. Non-linear image registration for correction of motion artifacts during optical imaging of human hearts. In: Conf Proc CCECE/CCGEI, pp. 1729–1732.
White, E., Le Guennec, J.Y., Nigretto, J.M., Gannier, F., Argibay, J.A., Garnier, D., 1993. The effects of increasing cell length on auxotonic contractions; membrane potential and intracellular calcium transients in single guinea-pig ventricular myocytes. Exp. Physiol. 78, 65–78.
Yue Yu, T., Syeda, F., Holmes, A., Osborne, B., Dehghani, H., Brain, K.L., Kirchhof, P., Fabritz, L., 2014. An automated system using spatial oversampling for optical mapping in murine atria. Development and validation with monophasic and transmembrane action potentials. Prog. Bio. Mol. Biol. 115 (2-3), 340–348. http://dx.doi.org/10.1016/j.pbiomolbio.2014.07.012.
Yasuda, S.I., Sugiura, S., Kobayakawa, N., Fujita, H., Yamashita, H., Katoh, K., Saeki, Y., Kaneko, H., Suda, Y., Nagai, R., Sugi, H., 2001. A novel method to study contraction characteristics of a single cardiac myocyte using carbon fibers. Am. J. Physiol. Heart Circ. Physiol. 281, H1442–H1446.
Zabel, M., Koller, B.S., Sachs, F., Franz, M.R., 1996. Stretch-induced voltage changes in the isolated beating heart: importance of the timing of stretch and implications for stretch-activated ion channels. Cardiovasc. Res. 32, 120–130.
Zeng, T., Bett, G.C., Sachs, F., 2000. Stretch-activated whole cell currents in adult rat cardiac myocytes. Am. J. Physiol. Heart Circ. Physiol. 278, H548–H557.
Zhang, Y., Sekar, R.B., McCulloch, A.D., Tung, L., 2008. Cell cultures as models of cardiac mechanoelectric feedback. Prog. Biophys. Mol. Biol. 97, 367–382.

EUROPEAN SOCIETY OF CARDIOLOGY®

European Journal of Heart Failure (2014)
doi:10.1002/ejhf.164

Adding the acetylcholinesterase inhibitor, donepezil, to losartan treatment markedly improves long-term survival in rats with chronic heart failure

Meihua Li*, Can Zheng, Toru Kawada, Masashi Inagaki, Kazunori Uemura, and Masaru Sugimachi

Department of Cardiovascular Dynamics, National Cerebral and Cardiovascular Center, Osaka, Japan

Received 17 June 2014; revised 2 July 2014; accepted 4 July 2014

Aims Modulation of vagal tone using electrical vagal nerve stimulation or pharmacological acetylcholinesterase inhibition by donepezil exerts beneficial effects in an animal model of chronic heart failure (CHF). Considering different treatment mechanisms underlying renin–angiotensin system (RAS) suppression and parasympathetic activation, we hypothesized that parasympathetic activation together with RAS inhibition could attenuate CHF progression. To test this hypothesis, we investigated the therapeutic effects of a combination of donepezil and losartan in CHF rats with extensive myocardial infarction (MI).

Methods and results Rats ($n=85$) that had survived extensive MI were implanted with a blood pressure transmitter and were randomly assigned to receive either a combination of donepezil and losartan (DLT group) or losartan alone (LT group). Compared with the LT group, the DLT group showed a significantly lower heart rate without hypotension. DLT therapy further improved 280-day overall survival relative to the LT group (31% vs. 8%, $P=0.022$) by preventing cardiac dysfunction (LV dP/dt_{max}, 4064 ± 170 vs. 3430 ± 117 mmHg/s, $P<0.01$; LV end-diastolic pressure, 17 ± 2 vs. 22 ± 2 mmHg, $P<0.05$). DLT therapy was also associated with lower plasma BNP and catecholamine levels, lower cardiac angiotensin II concentrations, and higher capillary density in the peri-infarct region.

Conclusions Combined treatment with donepezil and losartan prevented the progression of cardiac dysfunction and improved the long-term survival of CHF rats with extensive MI, suggesting that this combination could be a novel pharmacotherapy for severe CHF.

Keywords Donepezil • Losartan • Heart failure • Myocardial infarction • Survival

Introduction

Chronic heart failure (CHF) is characterized by overactivity of the sympathetic nervous system and the renin–angiotensin system (RAS), and reduced activity of the parasympathetic nervous system.[1–4] Currently, treatment for CHF has been centred on reducing the sympathetic effects, leading to the widespread clinical use of pharmacotherapeutic agents, including beta-blockers,[5–7] ACE inhibitors, and ARBs,[8–10] which have demonstrated favourable long-term effects on mortality and morbidity. The combination of beta-blockers with an ACE inhibitor and/or an ARB was subsequently recommended by the American Heart Association, and this combination is presently considered a standard therapy for CHF.[11] Despite these potent drugs, CHF is one of the main reasons for hospitalization.[12] Patients with CHF have low quality of life, and their mortality rate remains high.

Because diminished parasympathetic activity is another important independent risk factor underlying CHF[13] and myocardial

*Corresponding author. Department of Cardiovascular Dynamics, National Cerebral and Cardiovascular Center, 5-7-1 Fujishirodai, Suita, Osaka 565-8565, Japan. Tel: +81 6 6833 5012, ext. 2427, Fax: +81 6 6835 5403, Email: limeihua@ncvc.go.jp

infarction (MI),[14] restoring parasympathetic activity could be an alternative treatment for CHF. As a first step towards developing a therapeutic strategy targeting the parasympathetic system, we demonstrated that electrical vagal nerve stimulation (VNS) markedly improved the long-term survival of CHF rats with extensive MI, by preventing the progression of pumping failure and cardiac remodelling.[15,16] This treatment strategy had been evaluated in clinical trials and was shown to be feasible and beneficial for CHF patients.[17,18] Nonetheless, because VNS is an invasive approach, further large-scale and long-term clinical studies are necessary to verify its safety and effectiveness. Furthermore, the cost of the stimulation device and implantation surgery may become limiting factors for its standard clinical use. Since the efferent vagal nerve activity is transmitted by acetylcholine, drugs that increase local acetylcholine concentration can yield a bradycardic effect similar to that of VNS.[19,20] Previously, we found that administration of donepezil, an acetylcholinesterase inhibitor used in the palliative treatment of Alzheimer's disease, significantly increased vagal tone[21] and improved long-term survival in rats with extensive MI.[22]

Any potential therapy to be considered for clinical translation should be examined for its compatibility with established treatments. Considering that different treatment mechanisms are presumably involved in RAS suppression and parasympathetic activation, we hypothesized that parasympathetic activation together with RAS inhibition could attenuate CHF progression. RAS inhibition by a specific ARB, such as losartan, has been shown to prevent ventricular remodelling and improve the prognostic outcome in CHF, and ARBs are prescribed as routine drugs for CHF patients. In the present study, we investigated whether donepezil is effective in further suppressing cardiac dysfunction and improving long-term survival when administered in combination with losartan in rats with extensive MI.

Methods

The care and use of the animals were in strict accordance with Directive 2010/63/EU of the European Parliament and the Guiding Principles for the Care and Use of Animals in the Field of Physiological Sciences, which have been approved by the Physiological Society of Japan. All protocols were reviewed and approved by the Animal Subject Committee in the National Cerebral and Cardiovascular Center.

Experimental heart failure

Extensive MI was induced by occluding the proximal left coronary artery in male Sprague–Dawley rats ($n = 180$; body weight: 250–280 g; SLC, Hamamatsu, Japan) under halothane inhalation anaesthesia, as described previously (3% at induction and 1.2% during surgery).[15,22] Approximately 50% ($n = 95$) of the animals with extensive MI survived beyond the first 24 h. One week later, we measured LVEF by echocardiography after inhalation of the anaesthetic halothane (1%), and those rats ($n = 85$) with EF <40% were enrolled in this study. We confirmed the infarct size by post-mortem examination.

Study design

At 2 weeks after extensive MI, the surviving rats were randomly assigned to receive treatment with a combination of donepezil and losartan (DLT group, $n = 41$) or treatment with losartan alone (LT group, $n = 40$) for remodelling and prognosis studies (*Figure 1A*). Donepezil (Eisai, Inc., Tokyo, Japan) was administered by dissolving the drug in drinking water to a concentration of 50 mg/L. The dosage of donepezil (5 mg/kg/day) was chosen to decrease the heart rate (HR) by 20–30 b.p.m. in MI rats. Losartan (LKT Laboratories, Inc., St. Paul, MN, USA) was administered by admixing the drug into food pellets, at a dose of 10 mg/kg/day during the first 2 weeks, then increased to 30 mg/kg/day throughout the study period (*Figure 1B*). The dosages of donepezil and losartan were determined by a preliminary study as the maximum levels that did not obviously affect daily food consumption or normal growth in MI rats.

Telemetric measurements of blood pressure and heart rate

One week after inducing extensive MI, we surgically implanted a blood pressure (BP) transmitter (TA11PA-C40, DSI, St. Paul, MN, USA) after inhalation of the anaesthetic halothane (3% at induction and 1.2% during surgery) in 32 CHF rats for the remodelling study, in accordance with previously described procedures.[15,22] The catheter was inserted into the abdominal aorta, and the transmitter was positioned in the abdomen. The BP and HR data were recorded continuously in freely moving animals. The recording was sampled at 500 Hz.

Haemodynamic measurements under anaesthesia

After the 6-week treatment, we conducted an acute haemodynamic study in the surviving CHF rats (LT, $n = 13$; DLT, $n = 14$) under anaesthesia (3% induction, 1.2% surgery, and 0.6% halothane during data recording). Left ventricular and arterial pressures were measured with a 2 Fr catheter-tip micromanometer (SPC-320, Millar Instruments, Inc., Houston, TX, USA), right atrial pressure was measured with a fluid-filled transducer, and aortic flow was measured by a transonic flow probe, as described previously.[15] All the signals were digitized at a rate of 500 Hz for 5 min. After completing the haemodynamic measurements, blood samples were collected from the right carotid artery, and all rats were sacrificed with an overdose of i.v. sodium pentobarbital (100 mg/kg). The heart was excised for weighing, and frozen heart samples and 4% phosphate-buffered paraformaldehyde solution-fixed paraffin sections were prepared for subsequent analysis.

Neurohumoral study

Plasma catecholamine concentrations were measured by high-performance liquid chromatography with electrochemical detection after alumina adsorption. Plasma levels of BNP, arginine vasopressin (AVP), and angiotensin II (Ang II), and cardiac Ang II concentration were determined using enzyme-linked immunosorbent assay (ELISA). For details, see the Supplementary material online, *Methods*.

Immunohistochemistry and microvessel density

Biventricular sections (4 μm thickness) were deparaffinized, placed in citrate buffer, and heated in an autoclave to enhance specific immune staining. The sections were incubated overnight with rabbit antihuman von Willebrand factor (vWF) polyclonal antibody at 4 °C and were then incubated with Alexa 633-conjugated goat antirabbit IgG

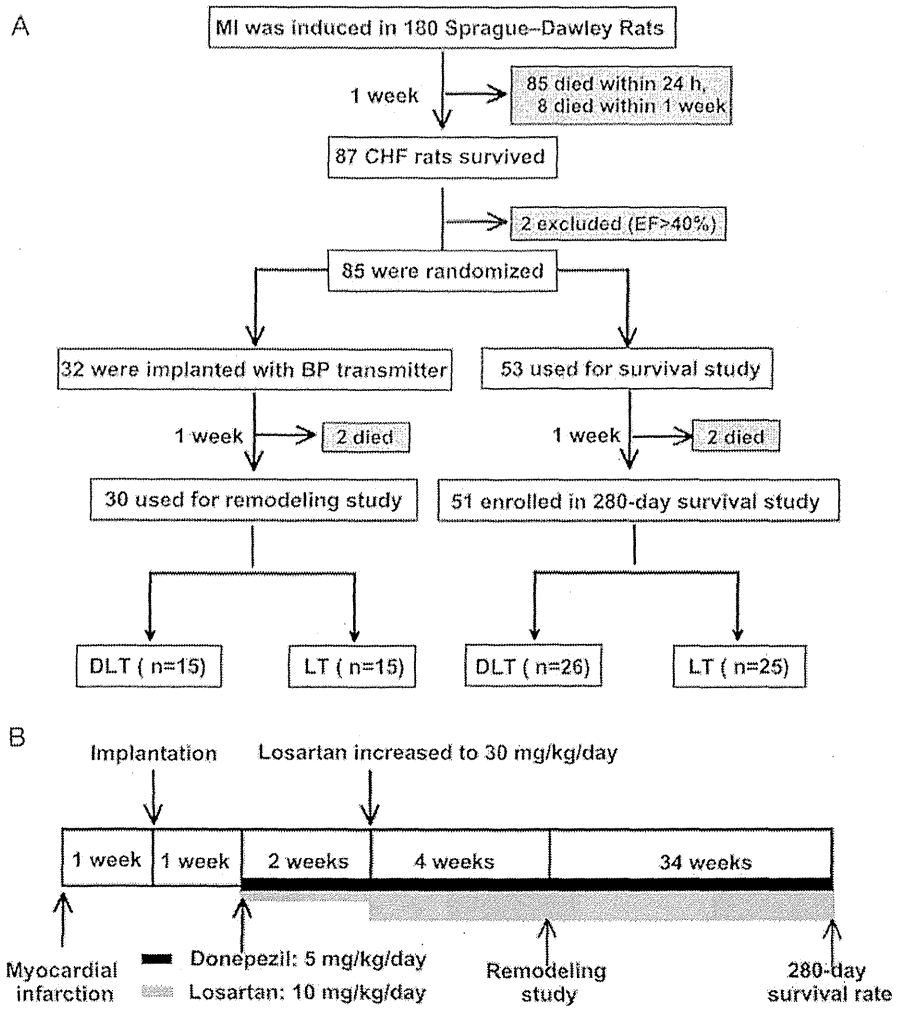

Figure 1 Schematic description of study design and timeline. (*A*) Study design of combined donepezil and losartan therapy in rats with chronic heart failure (CHF). The surviving CHF rats were randomly assigned to receive treatment with a combination of donepezil and losartan (DLT group) or to treatment with losartan alone (LT group) for remodelling and prognosis studies. (*B*) Study events and timeline. MI, myocardial infarction; EF, left ventricular ejection fraction; BP, blood pressure. At 2 weeks after extensive MI, donepezil (5 mg/kg/day) was administered by dissolving the drug in drinking water. Losartan was administered by admixing the drug into food pellets at a dose of 10 mg/kg/day during the first 2 weeks and increasing the dose to 30 mg/kg/day throughout the study period.

for microvessel analysis. Fluorescence of Alexa 633 was observed with a laser scanning microscope. Capillary vessels in the peri-infarct area, excluding the scar region, were counted using a laser scanning microscope system at × 20 magnification. Data obtained from high-power fields were averaged and expressed as the number of capillary vessels. Immunohistochemical double staining of Ang II type 1 (AT_1) receptors and smooth muscle actin (SMA) was performed in the sections. For details, see Supplementary materials online, *Methods*.

Western blotting and detection of proteins

For the western blotting investigation, a normal control group (N) and a CHF group without treatment (UT, 8 weeks post-MI) were analysed in addition to the DLT and LT groups. Frozen samples from the non-infarct left ventricle were homogenized for measuring cardiac Ang II concentrations by ELISA, and using western blotting for detecting AT_1 and AT_2 receptors. For details, see Supplementary materials online, *Methods*.

Determination of infarct size and histological examination

The heart was rapidly excised, rinsed to remove blood, weighed, and sliced. Biventricular sections (4 μm thickness) from the basal, middle, and apical portions were stained using Masson's trichrome method. Histological images were analysed using a frame grabber. Infarct size

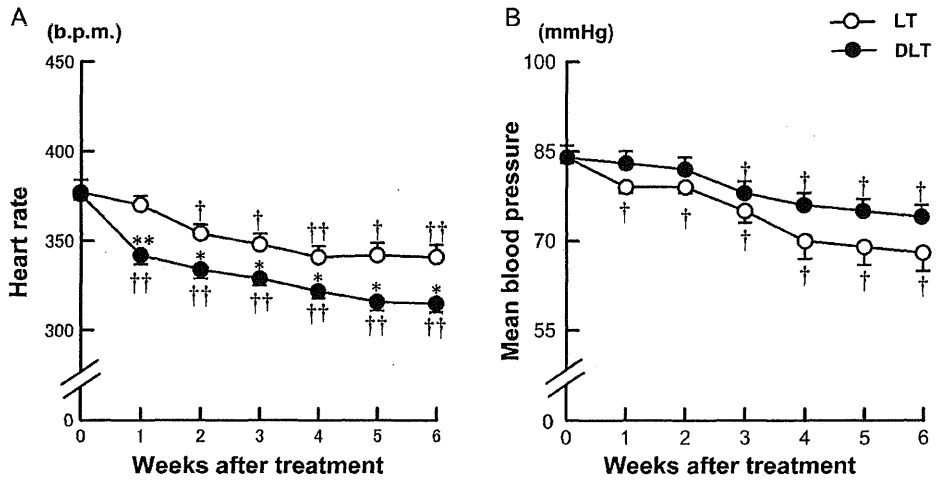

Figure 2 Telemetric haemodynamic changes in rats with chronic heart failure. (*A*) Mean heart rate (HR). (*B*) Mean blood pressure (MBP). Each point represents the average of 1 week's data from all animals in each group [losartan alone (LT), $n = 13$; donepezil + losartan (DLT), $n = 14$]. The average HR decreased significantly from the second week of treatment in both groups, but to a greater degree in the DLT group than in the LT group. The difference in HR between the DLT and LT groups reached ~30 b.p.m. at the sixth week of treatment (315 ± 6 b.p.m. vs. 341 ± 6 b.p.m., $P < 0.05$), while the MBP in the DLT group was not lower than that in the LT group (74 ± 6 mmHg vs. 68 ± 3 mmHg, *P*, non-significant). The values of the data points are given in the Supplementary material online, *Table S1*. Values are means ± SEM. $^{*}P < 0.05$; $^{**}P < 0.01$ vs. LT; $^{\dagger}P < 0.05$, $^{\dagger\dagger}P < 0.01$ vs. pre-treatment values (week 0) of each group by one-way ANOVA with repeated measures and post-hoc Dunnett's test.

was calculated from the three slices by dividing the sum of the endocardial lengths of infarcted regions by the sum of endocardial circumferences. The extent of myocardial fibrosis was evaluated using a light microscope at × 20 magnification. The myocardial fibrosis index was calculated from eight high-power fields in the non-infarct septum area in each rat.

Long-term survival study

To examine the outcomes of DLT and LT therapies, we evaluated survival over 280 days. The rats were inspected daily, and gross post-mortem examinations were conducted on dead rats. At the end of the observation period, surviving animals were sacrificed with an overdose (200 mg/kg) of sodium pentobarbital, injected intraperitoneally. The heart was removed for the subsequent measurement of infarct size. The cause of death was classified as pump failure if oedema, extreme weight loss accompanied by panting over a 24 h period before death, or obvious pleural effusion were observed. Otherwise, the cause of death was classified as sudden cardiac death.

Statistical analysis

All values are expressed as mean ± standard error of the mean (SEM). For data from the haemodynamic and remodelling study, differences between the DLT and LT groups were tested using Student's *t*-test. Differences in HR and BP before and during the treatment in each group were examined using one-way analysis if variance (ANOVA) with repeated measures and post-hoc Dunnett's test. For the neurohumoral data, the Mann–Whitney U-test was used to compare differences between the DLT and LT groups. For the western blot, the differences among the four groups were examined using one-way ANOVA and the post-hoc Tukey test. Survival data are presented as Kaplan–Meier curves, and the effect of treatment on 280-day survival was analysed using a log-rank test. The differences were considered significant for $P < 0.05$.

Results

Telemetric haemodynamic measurements

The averaged HR decreased significantly from the second week of treatment in both groups, but to a greater degree in the DLT group than in the LT group (*Figure 2A*). The difference in HRs between the DLT and LT groups reached ~30 b.p.m. at the sixth week of treatment (315 ± 6 vs. 341 ± 6 b.p.m., $P < 0.05$), while the mean BP was not lower in the DLT than in the LT group [74 ± 6 vs. 68 ± 3 mmHg, *P*, non-significant (NS); *Figure 2B*].

Anaesthetic haemodynamics and cardiac remodelling

The haemodynamic and remodelling parameters measured at the eighth week after extensive MI are shown in *Table 1*. Although there were no significant differences between the two groups in the body weight, normalized biventricular weight, infarct size, mean arterial pressure, and HR, the DLT rats had a significantly higher cardiac index and maximum and minimum *dP/dt* of LV pressure. Right atrial pressure and LV end-diastolic pressure were lower in the DLT than in the LT rats. The prevention of cardiac dysfunction in the DLT rats

Table 1 Haemodynamic and remodelling parameters after 6 weeks of treatment in rats with chronic heart failure

	LT group ($n=13$)	DLT group ($n=14$)	*P*-value
BW, g	442 ± 15	457 ± 10	NS
HW, g/kg	2.60 ± 0.09	2.51 ± 0.06	NS
Infarct size, %	46 ± 1	47 ± 2	NS
MBP, mmHg	69 ± 3	75 ± 2	NS
HR, b.p.m.	289 ± 7	299 ± 8	NS
CI, mL/min/kg	127 ± 4	145 ± 6	<0.05
LVEDP, mmHg	22 ± 2	17 ± 2	<0.05
LV dP/dt_{max}, mmHg/s	3430 ± 117	4064 ± 170	<0.01
LV dP/dt_{min}, mmHg/s	2657 ± 123	3076 ± 137	<0.05
RAP, mmHg	2.01 ± 0.29	1.16 ± 0.27	<0.05

Values are means ± SEM.
BW, body weight; CI, cardiac index; DLT, donepezil + losartan; HR, heart rate, HW, biventricular weight normalized by body weight; LT, losartan alone; LVEDP, left ventricular end-diastolic pressure; LV dP/dt_{max}, maximum dP/dt of left ventricular pressure; LV dP/dt_{min}, minimum dP/dt of left ventricular pressure; MBP, mean arterial pressure; RAP, right atrial pressure; SEM, standard error of the mean.
P-value, significance of difference between LT and DLT groups assessed by Student's *t*-test. NS, not significant ($P > 0.05$).

was accompanied by a significantly decreased cardiac fibrosis index in the non-infarct septum (0.97 ± 0.09% vs. 1.22 ± 0.07%, $P < 0.05$; *Figure 3C*).

Response of neurohumoral levels to treatments

The plasma levels of norepinephrine, epinephrine, and BNP were significantly lower in the DLT than in the LT group (*Table 2*). Although plasma AVP and Ang II did not differ significantly between the two groups, the cardiac Ang II concentration in the DLT group was reduced by two-thirds compared with the LT group.

Microvascular immunohistochemistry

The immunohistochemical study showed a greater degree of neovascularization in the DLT group than in the LT group (*Figure 4A*). Quantitative analysis demonstrated that capillary density was significantly higher in the DLT than in the LT group (*Figure 4B*, 107 ± 5 vs. 58 ± 3 vessels/field, $P < 0.01$). Further immunohistochemical double staining with AT_1 and SMA showed less AT_1 receptor activity in the DLT than in the LT group (*Figure 4C*).

Angiotensin II type 1 and type 2 receptor expression

Cardiac AT_1 receptor expression (*Figure 5A*) was detected in the 43 and 85 kDa putative bands. The 85 kDa band is a dimer or a different *N*-glycosylation state of the AT_1 receptor.[23] Rats with MI showed no change in AT_1 43 kDa but had significantly greater AT_1 85 kDa expression than normal rats. LT treatment significantly suppressed AT_1 43 kDa without any effect on AT_1 85 kDa compared with untreated MI. DLT treatment significantly reduced AT_1 85 kDa expression but not AT_1 43 kDa (*Figure 5C*) compared with LT. Cardiac AT_2 receptor expression (*Figure 5B*), detected in the 48 and 62 kDa bands, did not differ significantly among the four groups (*Figure 5D*).

Long-term survival study

Rats with healed extensive MI ($n = 51$) were used in the long-term survival study. As shown in the Kaplan–Meier curves for 280-day all-cause mortality (*Figure 6*), the survival rate of CHF rats was markedly higher in the DLT group than in the LT group from day 140 (92% vs. 64%, $P = 0.014$) to the end of the observation period. Eight rats (31%) in the DLT group vs. only 2 rats (8%) in the LT group survived until 280 days ($P = 0.022$). The median survival was 167 days in the LT group and 227 days in the DLT group. The cause of death was further analysed. Pump failure accounted for 30% of deaths in the DLT group and 81% of deaths in the LT group, indicating that DLT therapy had a significant effect in preventing pump failure death (Supplementary material online, *Figure S1A*, 30% vs. 81%, $P = 0.009$). However, the incidence of sudden cardiac death did not differ between the DLT (57%) and LT (56%) groups (Supplementary material online, *Figure S1B*, $P = 0.506$). Even after the rats that survived until the end of the study period were excluded, the LT and DLT groups showed no significant difference in either normalized biventricular weight (3.04 ± 0.09 vs. 2.98 ± 0.09 g/kg) or infarct size (48% ± 3% vs. 48% ± 1%).

Discussion

This study has shown that treatment with the DLT combination in severe CHF rats (i) markedly improved 280-day survival; (ii) ameliorated cardiac dysfunction; and (iii) decreased HR without significantly altering mean BP, compared with the LT group. The DLT combination also (iv) significantly suppressed plasma catecholamine, BNP, and cardiac Ang II levels and (v) improved histological features relative to the LT group. These findings suggest that pharmacological restoration of vagal tone by an acetylcholinesterase inhibitor, donepezil, and inhibition of RAS by losartan may work co-operatively to enhance cardioprotective beneficial effects in CHF rats with extensive MI.

Previously obtained knowledge

The study design and protocol of the present study are in line with those of our previous report,[22] the results of which are summarized in brief. We randomized MI-induced CHF rats to donepezil treatment (DT) or no treatment (UT) groups 14 days after the induction of MI. Donepezil was administered dissolved in drinking water (5 mg/kg/day). Compared with the UT group, DT therapy significantly prevented LV remodelling and dysfunction, and reduced neurohumoral activation. This prevention was associated with a significant improvement in survival at 140 days in the DT

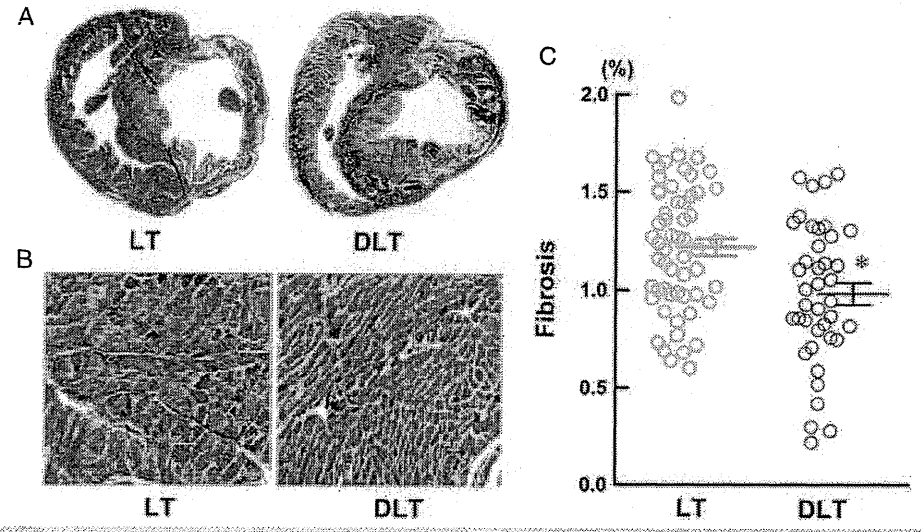

Figure 3 Masson's trichrome staining on ventricle slides of rats with chronic heart failure. (*A*) Representative biventricular sections of extensive myocardial infarction. (*B*) Representative image of the myocardial fibrosis in the non-infarct septum. (*C*) Myocardial fibrosis index in the septum area [1.22 ± 0.07%; losartan alone (LT), $n = 7$, 56 fields vs. 0.97 ± 0.09%; donepezil + losartan (DLT), $n = 5$, 40 fields]. Values are means ± SEM. *$P < 0.05$ vs. LT by Student's *t*-test.

group (54%) compared with the UT group (29%, $P = 0.03$). These values will be referred to in the following discussion.

Possible treatment mechanisms involved in donepezil + losartan therapy

We assessed stress-free haemodynamics of CHF rats by telemetry. DLT therapy reduced ambulatory HR compared with LT therapy, while the mean BP in the DLT group was similar to that in the LT group (*Figure 2*). These results are partly consistent with those of a previous study, in which parasympathetic activation by donepezil significantly reduced HR but did not affect mean BP.[22] Prevention of cardiac dysfunction, as evidenced by the increased cardiac index (*Table 1*), may also have contributed to the maintenance of mean BP, yielding arterial baroreflex-mediated inhibition of sympathetic nerve activity and reduction of HR.[24] A prolonged cardiac cycle is beneficial in enhancing and maintaining cardiac function, by decreasing myocardial oxygen consumption, increasing coronary flow, and increasing ventricular filling volume.[25] Clinical studies also indicate that HR is an independent risk factor in CHF,[13] and antiadrenergic treatment by beta-blockers is a routine prescription for most CHF patients.[26] In a recent clinical trial, SHIFT, HR reduction with ivabradine improved clinical outcomes in CHF patients.[27] Therefore, the bradycardic effect seen in the DLT group may be one of the important factors for preventing cardiac dysfunction.

While both the DLT combination and beta-blockers exert bradycardic effects, the former may have a potential advantage compared with the latter. Because adrenergic receptors exist on both the sinus node and cardiac myocytes, beta-blockers not only decrease HR but also suppress ventricular contractility. Hence, due to these negative inotropic effects, beta-blockers may not be suitable for patients with decompensated conditions or pre-existing myocardial dysfunction, since the maintenance of cardiac output in such patients depends in part upon sympathetic drive. On the other hand, because of the scarce distribution of acetylcholine-dependent potassium channels in the ventricles, vagal activation shows less direct negative inotropic effects.[28,29] Moreover, because pre-ganglionic fibres are cholinergic, donepezil

Table 2 Neurohumoral variables in plasma and tissue after 6 weeks of treatment in rats with chronic heart failure

	LT group ($n = 13$)	DLT group ($n = 14$)	*P*-value
Plasma norepinephrine, pg/mL	1522 ± 273	931 ± 104	<0.05
Plasma epinephrine, pg/mL	2375 ± 386	1187 ± 138	<0.01
Plasma BNP, pg/mL	391 ± 8	358 ± 10	0.01
Plasma AVP, pg/mL	293 ± 19	278 ± 22	NS
Plasma Ang II, pg/mL	34 ± 4	50 ± 8	NS
Cardiac Ang II, pg/g protein	121 ± 34	42 ± 18	<0.05

Values are means ± SEM.
Ang II, angiotensin II; AVP, arginine vasopressin; DLT, donepezil + losartan; LT, losartan alone; SEM, standard error of the mean.
P-value, significance of difference between LT and DLT groups assessed by the Mann–Whitney U-test. NS, not significant ($P > 0.05$).

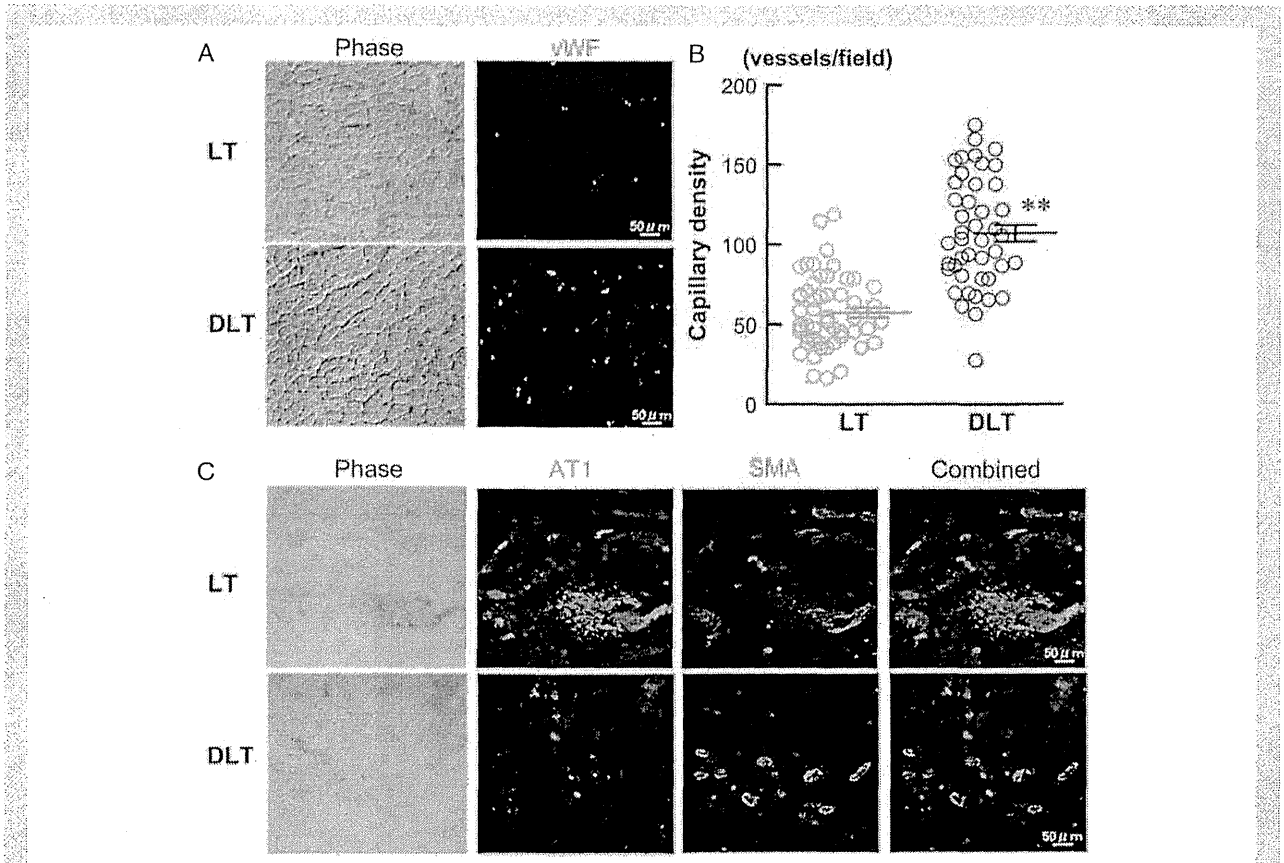

Figure 4 Immunohistochemical and microvessel analysis in the peri-infarct area of rats with chronic heart failure. (*A*) Representative micrographs of von Willebrand factor (vWF, red) immunostaining. Phase: phase-contrast image. (*B*) Quantitative analysis of capillary density. [58 ± 3; losartan alone (LT), $n = 6$, 54 fields vs. 107 ± 5 vessels/field; donepezil + losartan (DLT), $n = 5$, 44 fields]. Values are means ± SEM. $^{**}P < 0.01$ vs. LT by Student's *t*-test. (*C*) Immunofluorescent expression of cardiac angiotensin II type 1 (AT_1) receptor (green) and smooth muscle actin (SMA, red) in the ischaemic border zone. The vascular AT_1 receptor appeared more active in the LT ($n = 3$) than in the DLT ($n = 3$) group.

can theoretically increase synaptic transduction in both sympathetic and parasympathetic nerves.[30,31] Therefore, donepezil may increase synaptic acetylcholine and reduce HR, with less negative effects on ventricular contractility. In the DLT group, the finding of decreased HR without significant effects on mean BP may partly support this interpretation; this phenomenon is similar to the effects of ivabradine treatment that showed HR reduction without negative inotropism in CHF.[27]

In addition to the above-mentioned haemodynamic-related mechanisms, the cholinergic anti-inflammatory pathway[32,33] may be another important mechanism for cardiac protection in DLT therapy.[34–36] In a previous study, we found that DT rats had lower levels of inflammatory cytokines in the heart, liver, and lung tissue compared with UT rats,[22] and this effect of donepezil may partly account for the suppression of myocardial interstitial fibrosis in the DLT group compared with the LT group (*Figure 3C*). Furthermore, the cholinergic angiogenic pathway[37] might lead to increased capillary density in the peri-infarct region (*Figure 4B*). Abundant vascularization is the basis or indicator of elastic myocardium,[38] and may have partially improved or preserved cardiac function, resulting in the improved outcomes in the DLT group compared with the LT group.

Effects of donepezil + losartan therapy on cardiac remodelling and neurohumoral factors

Normalized biventricular weight, an indicator of cardiac hypertrophy, was not significantly lower in the DLT group than in the LT group. Because losartan and other ARB drugs exhibit potent anticardiac remodelling effects[39–42] with respect to cardiac hypertrophy, there may not have been much room for further improvement by the addition of donepezil. However, histological and neurohumoral assays might provide new insights into the understanding of DLT therapy, as follows. The DLT group showed lower Ang II levels in cardiac tissue compared with the LT group (*Table 2*). Donepezil inhibits local Ang II production through a

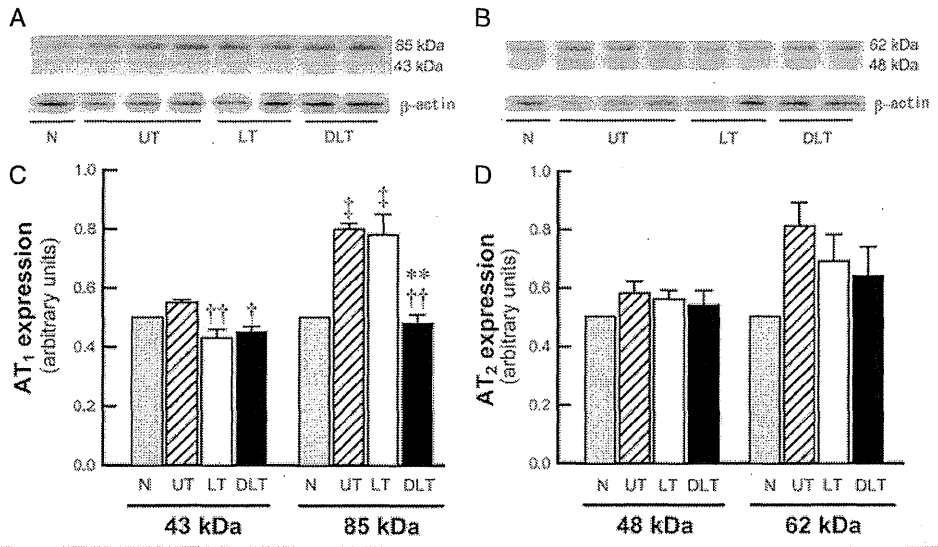

Figure 5 Western blotting analyses. (*A*) Representative immunoblots of homogenates of the left ventricle from rats with chronic heart failure (CHF) probed with polyclonal angiotensin II type 1 (AT_1) receptor antibody. (*B*) Polyclonal angiotensin II type 2 (AT_2) receptor antibody. (*C*) Densitometry analysis of AT_1 and (*D*) AT_2 receptors obtained from normal controls (N, $n=5$), untreated CHF (UT, 8 weeks post-myocardial infarction, $n=5$), losartan alone (LT; $n=7$) and donepezil + losartan (DLT; $n=7$) rats. Values are means ± SEM. †$P<0.05$, ††$P<0.01$ vs. UT; ‡$P<0.01$ vs. N; **$P<0.01$ vs. LT by one-way ANOVA and the post-hoc Tukey test.

heart-specific chymase-dependent pathway.[43] Along with increasing capillary density, DLT therapy decreased vascular AT_1 receptor activity (*Figure 4C*), which may indicate that this receptor is directly involved in angiogenesis.[23] Further, the results of the protein detection assay showed that, although UT rats had no change in AT_1 43 kDa, they had significantly greater AT_1 85 kDa expression than normal rats; this finding is consistent with a previous report.[23] Losartan treatment significantly decreased the AT_1 43 kDa receptors compared with UT, a result similar to that of a previous report indicating that long-term ARB treatment caused down-regulation of AT_1 receptors.[41] Addition of donepezil induced down-regulation of the AT_1 85 kDa receptors (*Figure 5C*) compared with the LT group. The AT_1 85 kDa receptor is a dimer or a different *N*-glycosylation state that is necessary for the adequate delivery of the receptor from the endoplasmic reticulum to the plasma membrane.[23,44] Whether donepezil modulates this process directly or indirectly is unknown.

DLT therapy significantly reduced plasma catecholamine and BNP levels compared with LT therapy (*Table 2*). Therefore, this combination therapy would effectively retard the vicious circle of maladaptation in CHF, by augmenting vagal tone and suppressing chronic overactivity of the sympathetic nervous system and the RAS.

Effects of donepezil + losartan therapy on survival

In the present study, CHF rats with extensive MI were enrolled and followed for up to 280 days (294 days post-MI). We found

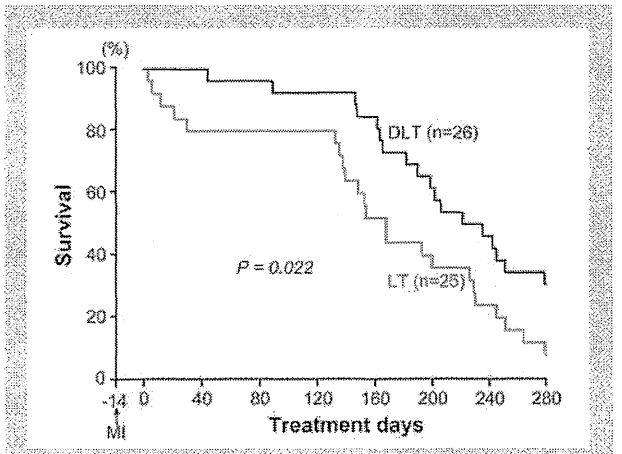

Figure 6 Kaplan–Meier survival curves of animals treated with losartan alone (LT) and donepezil + losartan combination (DLT). Treatment was started 14 days after myocardial infarction (MI). DLT significantly improved the 280-day survival rate compared with LT (31% vs. 8%, $P=0.022$, by log-rank test). The median survival for the LT group was 167 days, compared with 227 days for the DLT group.

that the median survival was 227 days in the DLT group and 167 days in the LT group. A significant difference in survival was detected from day 140 (*Figure 6*; 92% vs. 64%, $P=0.014$) to the end of the observation period (*Figure 6*; 31% vs. 8%, $P=0.022$). This result may indicate that DLT therapy conferred

better prognostic benefits, not only than losartan alone, but also than donepezil alone (DT, 54%; UT, 29%, at day 140).[22] Further analysis of the cause of death (Supplementary material online, *Figure S1*) demonstrated that adding donepezil reduced pump failure death (Supplementary material online, *Figure S1A*; 30% vs. 89%, $P = 0.009$) but not sudden cardiac death (Supplementary material online, *Figure S1B*; 57% vs. 56%, $P = 0.506$). This may suggest that the beneficial effect of donepezil treatment which started 2 weeks after MI was mainly exerted through the improvement of cardiac function, but the effects on arrhythmias and sudden cardiac death should be interpreted carefully with further investigation. From the viewpoint of 140-day survival, DLT therapy (92%) provided an equivalent treatment effect to that attained by VNS (86%) in CHF rats;[15] however, the differences in the protocols prevent us from inferring that the beneficial effects of DLT therapy are the same as those of VNS therapy.

Beta-blockers, ACE inhibitors, or ARBs have been reported to improve the prognosis of CHF rats with a small to moderate infarct size, but had no or less effect on long-term survival in rats with a large infarct size.[39,45,46] In agreement with these reports, only two rats (8%) in the LT group survived until 280 days in the present study. In contrast, eight rats (31%) in the DLT group survived until 280 days, demonstrating the additional beneficial effects obtained from the DLT combination for the treatment of severe CHF induced by a large MI.

Possible clinical implications

To the best of our knowledge, this study is the first to demonstrate the therapeutic efficacy of a combination of parasympathetic activation by donepezil and RAS inhibition by losartan in the treatment of CHF. In fact, since RAS inhibition by ACE inhibitors and/or ARBs has been established as a first-line therapy to prevent the progression of heart failure,[47] and donepezil has been clinically approved for the treatment of Alzheimer's disease, this drug combination could be considered as a novel therapeutic strategy for patients with severe CHF. Furthermore, a recent cohort study reported that use of a cholinesterase inhibitor reduced the risk of MI and death in subjects with Alzheimer's disease.[48] Future studies are warranted to evaluate this promising therapy in clinical settings. Based on its different mechanism of HR reduction, donepezil may be an alternative for those patients who are intolerant of beta-blocker therapy, or for those whose HR does not decrease adequately in response to beta-blockers. In addition, whether donepezil can be combined with the beta-blocker therapy for CHF should be examined in a further study.

Limitations

Although the drugs used in this study are clinically available, their mode of administration during clinical use in humans and in animal studies is different. In this study, the drugs were dissolved in drinking water (donepezil) or admixed in the diet (losartan). Because of their nocturnal habits, rats usually feed and drink frequently during the night (e.g. drinking 4–16 times daily). Several circulatory surges might have occurred due to donepezil absorbed from the drinking water. Therefore, the dynamics of drug metabolism in this animal model would be different from the clinical situation in which donepezil is taken once a day. In rat studies, the drug is usually dissolved in drinking water at a concentration of 50–150 times the clinical dose.[39,45] We selected the daily dose of donepezil for the rats to be almost 50 times the clinical dose used for Alzheimer's disease. It may be necessary to clarify whether this difference will influence the therapeutic effects of the drug.

Conclusions

This study demonstrates that a combination of donepezil and losartan has a marked protective effect against cardiac dysfunction, and improves long-term survival in CHF rats with extensive MI. We propose the pharmacological inhibition of acetylcholinesterase concomitant with ARB treatment as a novel therapeutic strategy for CHF patients.

Supplementary Information

Additional Supporting Information may be found in the online version of this article:

Appendix S1. Supplementary methods and results.

Figure S1. Survival rates were classified by the cause of death as either pump failure or sudden cardiac death.

Table S1. Weekly averaged hemodynamic measurements in rats with chronic heart failure at baseline and following treatment

Conflict of interest: none declared.

References

1. Packer M. The neurohormonal hypothesis: a theory to explain the mechanism of disease progression in heart failure. *J Am Coll Cardiol* 1992;**20**:248–254.
2. *Binkley PF, Nunziata E, Haas GJ, Nelson SD, Cody RJ. Parasympathetic withdrawal* is an integral component of autonomic imbalance in congestive heart failure: demonstration in human subjects and verification in a paced canine model of ventricular failure. *J Am Coll Cardiol* 1991;**18**:464–472.
3. Mann DL. Mechanisms and models in heart failure: a combinatorial approach. *Circulation* 1999;**100**:999–1008.
4. Braunwald E, Bristow MR. Congestive heart failure: fifty years of progress. *Circulation* 2000;**102**:IV14–IV23.
5. Gattis WA, O'Connor CM, Gallup DS, Hasselblad V, Gheorghiade M, IMPACT-HF Investigators and Coordinators. Predischarge initiation of carvedilol in patients hospitalized for decompensated heart failure: results of the Initiation Management Predischarge: Process for Assessment of Carvedilol Therapy in Heart Failure (IMPACT-HF) trial. *J Am Coll Cardiol* 2004;**43**:1534–1541.
6. McAlister FA, Wiebe N, Ezekowitz JA, Leung AA, Armstrong PW. Meta-analysis: beta-blocker dose, heart rate reduction, and death in patients with heart failure. *Ann Intern Med* 2009;**150**:784–794.
7. Pepper GS, Lee RW. Sympathetic activation in heart failure and its treatment with beta-blockade. *Arch Intern Med* 1999;**159**:225–234.
8. Packer M, Poole-Wilson PA, Armstrong PW, Cleland JG, Horowitz JD, Massie BM, Rydon L, Thygesen K, Uretsky BF. Comparative effects of low and high doses of the angiotensin-converting enzyme inhibitor, lisinopril, on morbidity and mortality in chronic heart failure. ATLAS Study Group. *Circulation* 1999;**100**:2312–2318.
9. Flather MD, Yusuf S, Køber L, Pfeffer M, Hall A, Murray G, Torp-Pendersen C, Ball S, Pogue J, Moye L, Braunwald E. Long-term ACE-inhibitor therapy in patients with heart failure or left-ventricular dysfunction: a systematic overview of data from individual patients. ACE-Inhibitor Myocardial Infarction Collaborative Group. *Lancet* 2000;**355**:1575–1581.